Measurement 257 (2026) 118498

Contents lists available at ScienceDirect

Measurement

journal homepage: www.elsevier.com/locate/measurement

A novel approach to reliable SPT hammer energy measurement using FVCD method with dual-instrumentation and visual measurement validation

M.E. Yadhunandan [a], Panjamani Anbazhagan [a,*]

[a] Department of Civil Engineering, Indian Institute of Science, Bangalore 560012, India

ARTICLE INFO

Keywords:
Standard Penetration Test (SPT)
Hammer energy measurement
Energy Transfer Ratio (ETR)
Sampler penetration
Visual measurement

ABSTRACT

Accurate hammer energy measurement is crucial in the Standard Penetration Test (SPT). Estimating Energy Transfer Ratio (ETR) using the FV method is widely accepted, where a key factor is the duration considered for integration. Traditionally, this duration is defined by the 'tension cutoff'; however, this fixed time window is often inadequate for short rod lengths, as reflected waves return before complete energy transfer occurs. Moreover, identifying the arrival of reflected tensile waves is difficult in typical force and acceleration data. In practice, durations exceed the theoretical cutoff. Additionally, some studies have reported ETR at both anvil and sampler levels, but these lacked focus on ETR duration, used limited laboratory tests, and lacked substantial field data. This study, for the first time, used two instrumented rods at the anvil and sampler levels in both full-scale laboratory and field SPT setups to record wave behaviour across rigs, soil types, and a wide range of N-values using the SPT HEMA. This paper proposes a novel method- Force or Velocity Change Direction (FVCD), which defines a dynamic time window based on the first sign reversal in force or velocity, whichever occurs first. A force sign change indicates a reflected tensile wave; a velocity sign change shows particle motion reversal due to reflections. ETR from the FVCD method is validated through visual measurement using the High-Speed Camera with Circular targets at both levels. The FVCD method significantly improves the reliability of ETR estimation, especially in short-rod cases, by providing measurements directly linked to sampler penetration.

1. Introduction

The Standard Penetration Test (SPT) is a widely used in-situ test for evaluating soil properties in geotechnical engineering. It offers both soil resistance and samples simultaneously at the specific test depth. The SPT-N value (representing the number of hammer blows required for sampler penetration for the last 30 cm out of the overall 45 cm penetration into the soil) is a critical parameter for estimating various static and dynamic soil properties. However, despite its widespread use, the accuracy of the SPT-N value is susceptible to many errors from variations in the SPT practice, equipment, and component setup [1]. Significant variations arise from differences in SPT equipment components, such as the hammer, anvil, guide rod, drill rod, and the vertical alignment of the drill rod assembly. These components can vary significantly based on equipment and site-specific conditions. To mitigate these errors, several corrections are applied to measured N values as recommended in various international standards. ASTM D3740-19 [2] outlines general standardisation practices for soil test agencies. IS 2131:1981 [3] provides the SPT procedure and suggests overburden and dilatancy corrections. ASTM D4633-16 [4] provides guidance on energy

Abbreviations: SPT, Standard Penetration Test; N value / N, Number of blows required for 30 cm penetration in SPT; N_{60}, Standardized SPT-N value corrected for 60% hammer energy efficiency; ETR, Energy Transfer Ratio; FV method, Force-Velocity Method; FVCD method, Force or Velocity Change Direction method (a method that considers the ETR calculation duration from the beginning of stress wave propagation until either force or velocity first changes direction from positive to negative); SPT HEMA, Standard Penetration Test Hammer Energy Measurement Apparatus; HSC, High-Speed Camera; HSCCT, High-Speed Camera with Circular Target; EFV, Energy from Force-Velocity method; PE, Potential Energy; F(t), Time-dependent Force; V(t), Time-dependent Particle Velocity; L, Length of Drill Rod; c, Wave speed in Drill Rod; 1D, One-Dimensional; IS, Indian Standard; ASTM, American Society for Testing and Materials; BS EN ISO, British Standard European Norm International Organization for Standardization; DAQ, Data Acquisition system; SD, Standard Deviation; PDF, Probability Density Function; CI, Confidance Interval; P value, Probabiliry value used to test statistical significance; Cohen's d_s, Effect size used to indicate the standardized difference between two means; Pooled SD, Combined standard deviation for two groups.

* Corresponding author.
E-mail address: anbazhagan@iisc.ac.in (P. Anbazhagan).

https://doi.org/10.1016/j.measurement.2025.118498
Received 16 May 2025; Received in revised form 3 July 2025; Accepted 21 July 2025
Available online 23 July 2025

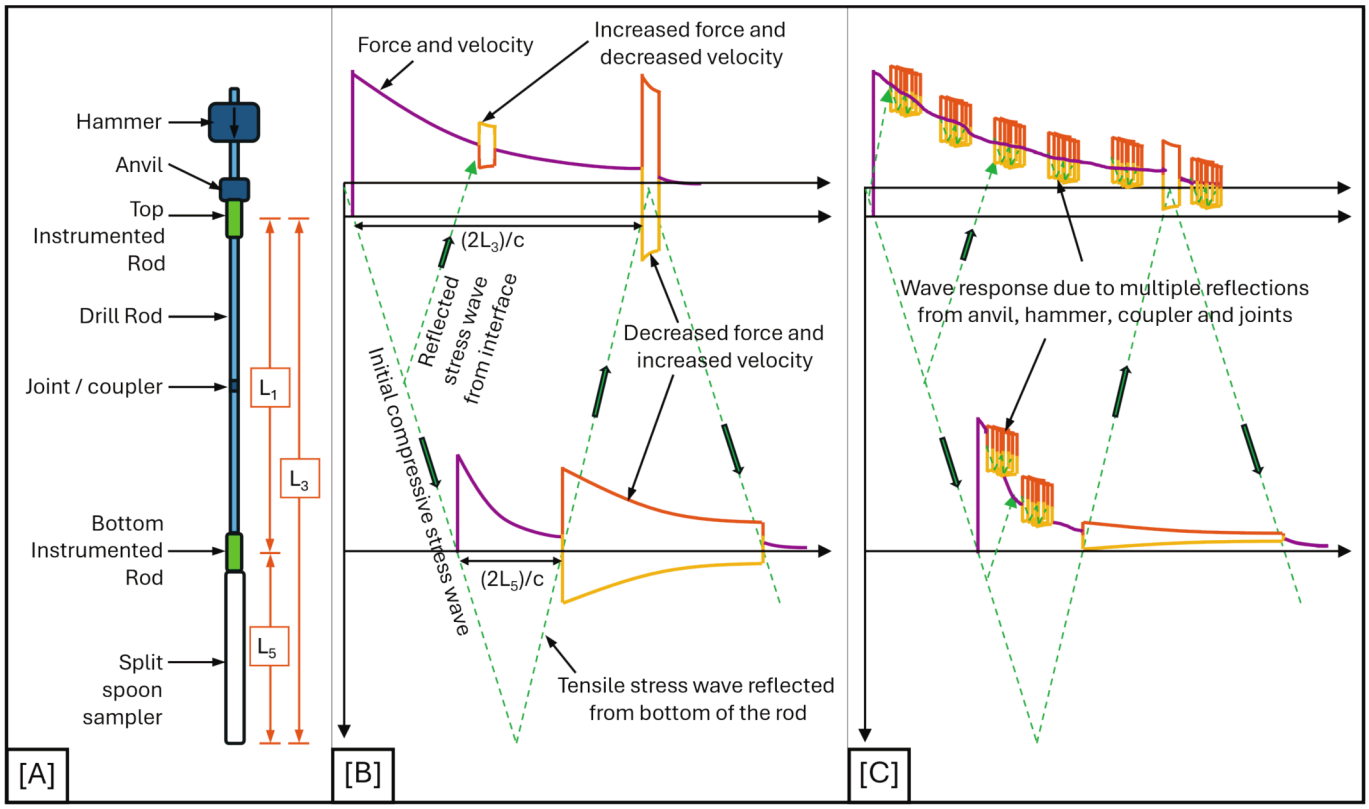

Fig. 1. [A] SPT schematic emphasising two instrumented rods at anvil and sampler level [B] Theoretical idealised wave response in SPT [22] [C] Idealized wave response considering joint/interface reflections.

measurement and corrections related to non-standard hammer weight and drop height. BS EN ISO 1377–9:1990 [5] and IS 9640:1980 [6] address the importance of standard sampler configuration, rod length, and borehole diameter corrections. BIS 1893 (Part 1):2016 [7] specifies detailed correction factors for SPT-N values, including corrections for overburden pressure, energy ratio, hammer weight and height of fall, rod length, sampler setup, and borehole diameter, especially for applications in earthquake-resistant design. Overburden and hammer energy corrections are the most predominant among these corrections, with the latter having the potential to eliminate most of the errors associated with SPT components [8,9]. Accurate hammer energy measurement and applying corrections to N values minimises these errors and ensures reliable SPT results. Several methods have been developed over the years to measure and evaluate hammer efficiency and address the influence of hammer energy on SPT reliability.

1.1. Hammer energy measuring methods

Before the 1970s, measurement of hammer energy efficiency in the SPT was not attempted. Due to energy losses from dropping mechanisms and variations in SPT components, researchers began to recognize the importance of hammer impact efficiency. Early studies on SPT hammer energy efficiency focused on comparing the actual hammer drop velocity to the theoretical standard velocity of 3.84 m/s [10]. Subsequent research introduced force transducers to measure force–time histories below the anvil, leading to the development of the Force-Square method (F^2 method) for energy estimation [11]. Despite its utility, the F^2 method has limitations, particularly in short rods (rod length less than 9 m) and when wave reflections occur at an impedance interface, rod coupling, or sampler-soil interface.

To address the limitations of the F^2 method, Sy and Campanella [12] introduced the Force-Velocity (FV) method, which uses force and acceleration measurements to calculate the hammer energy transfer (Joules) to drill rods. This method integrates the force multiplied by velocity over time, providing a more comprehensive assessment of hammer energy transfer. Abou-matar & Goble [13] refined the FV method by emphasising the proportionality between force and velocity for calculating the Energy Transfer Ratio (ETR, %) as shown in *Equation (1)*. The FV method considers energy transfer from the impact time until the reflected tensile wave arrives back at the measurement point (called a 'tension cut-off'), often represented as a '2L/c' time window (where, 'L' is the drill rod length from the measurement point just below the anvil to the bottom end of the sampler and 'c' is the wave speed in the drill rod). Additionally, the development of affordable, high-sensitivity accelerometers has since made the FV method widely adopted in SPT.

$$ETR(\%) = \frac{EFV}{PE} * 100 = \frac{\int_{t=0}^{t=2L/c} F(t) * V(t) dt}{PE} * 100 \quad (1)$$

Where: ETR = Energy Transfer Ratio (in %), EFV = Measured energy by FV method (in Joules), PE = Potential energy of the hammer impact (in Joules), t = stress wave travel time (in sec), L = drill rod length from the measurement point below the anvil to the bottom end of the sampler (in m), c = stress wave speed in drill rod (in m/sec), F(t) = measured force at anvil level (in N), V(t) = particle velocity obtained from integration of measured acceleration (in m/sec).

In addition to the commonly used F^2 and FV methods for SPT energy estimation, some advanced signal processing techniques, such as wavelet analysis and full-waveform inversion, have been explored for analyzing complex wave behavior. However, these methods are computationally intensive, require more sophisticated setups, and are unsuitable for routine field use in SPT. Additionally, there is no literature available applying these techniques specifically for estimating ETR from force and acceleration data in the SPT. Therefore, this study focuses on the practical and field-validated FV method and introduces a new and

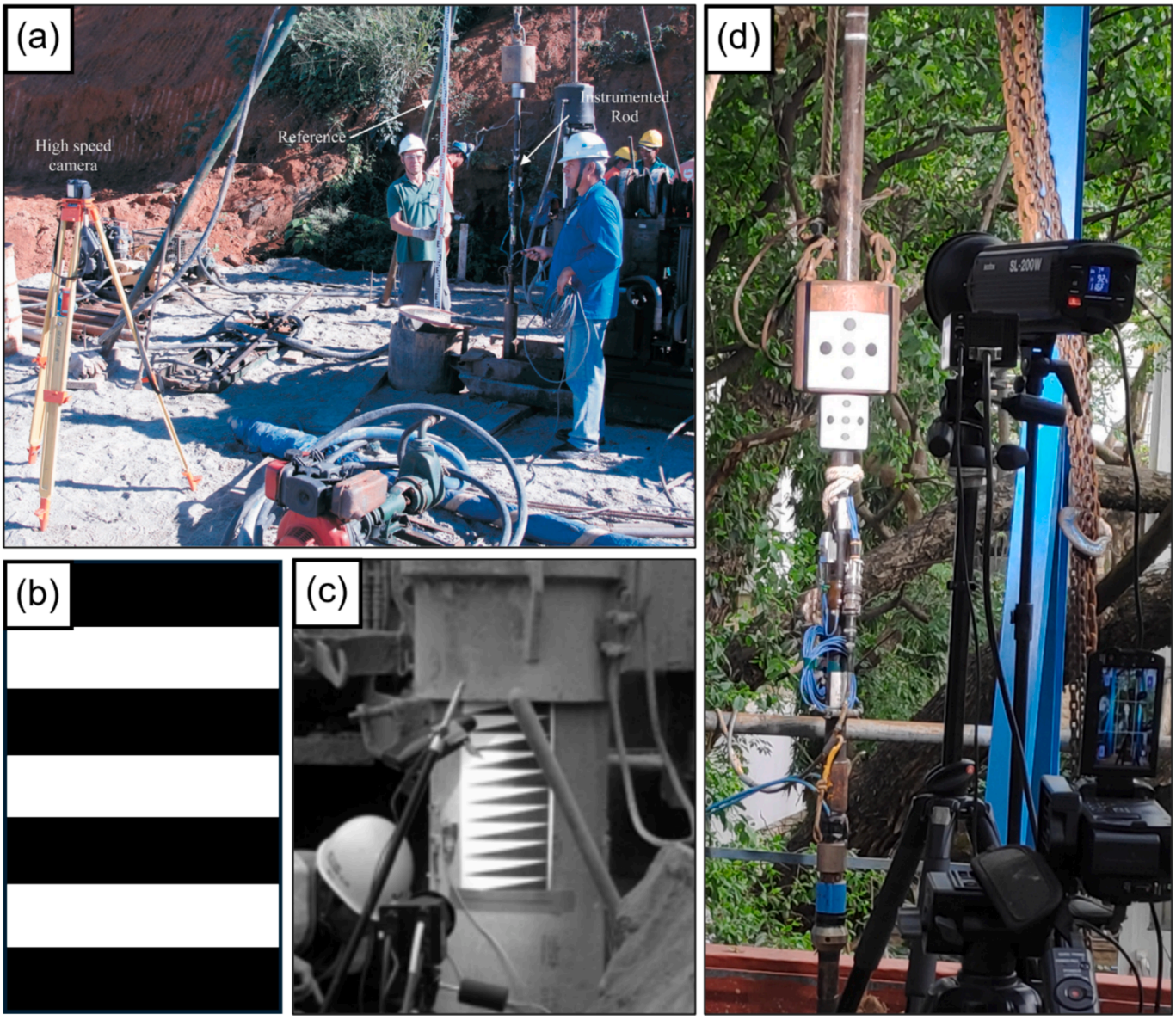

Fig. 2. Typical visual measurement target markings used in SPT: (a) Vertical staff [28], (b) Rectangular strip-shaped marker [29], (c) Triangular Strip Shaped marker [30], and (d) Circular target marker used in this study [32].

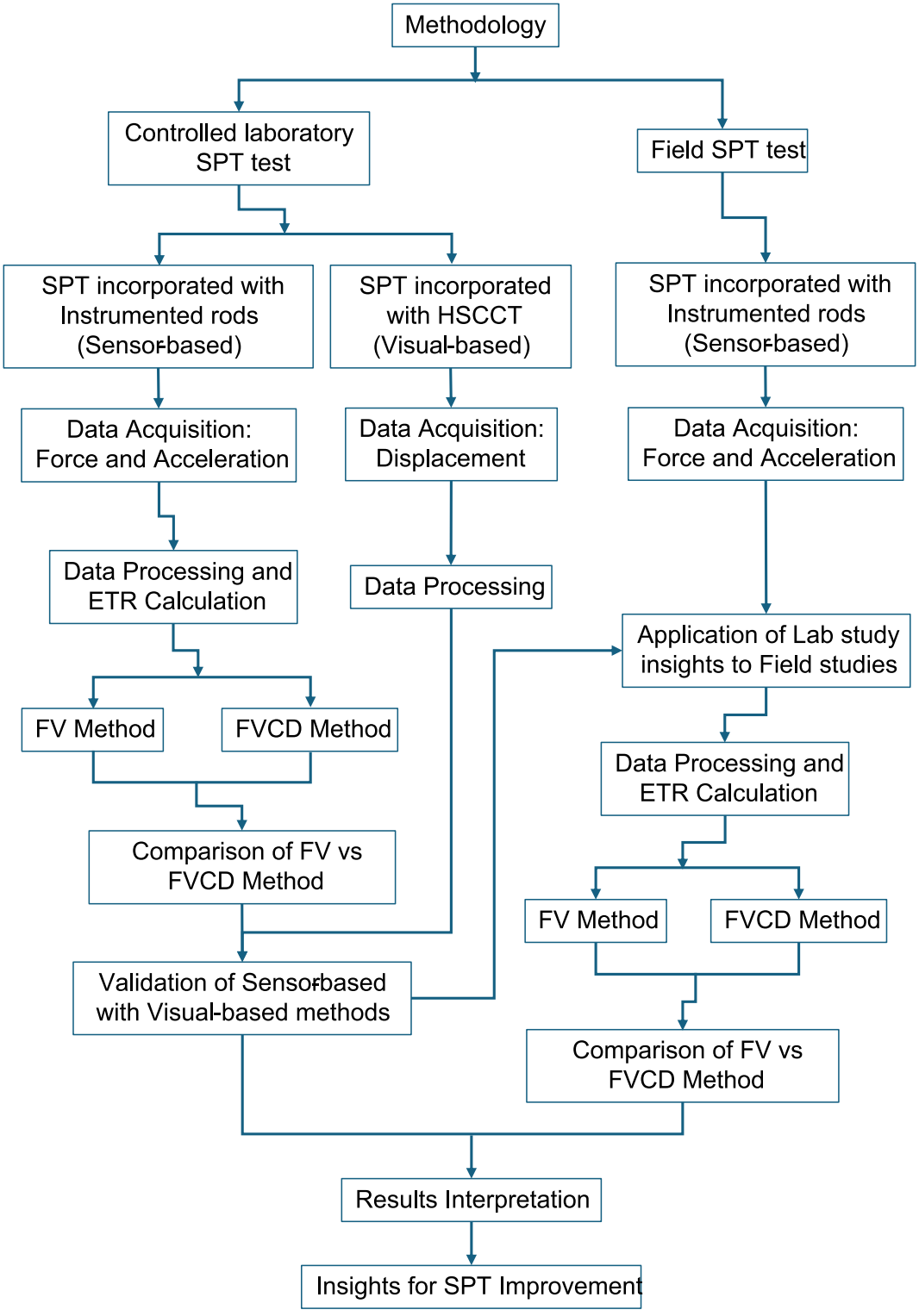

Fig. 3. The Methodology flowchart shows laboratory and field SPT testing, ETR calculation using FV and FVCD methods, validation with visual data, and final comparison and interpretation.

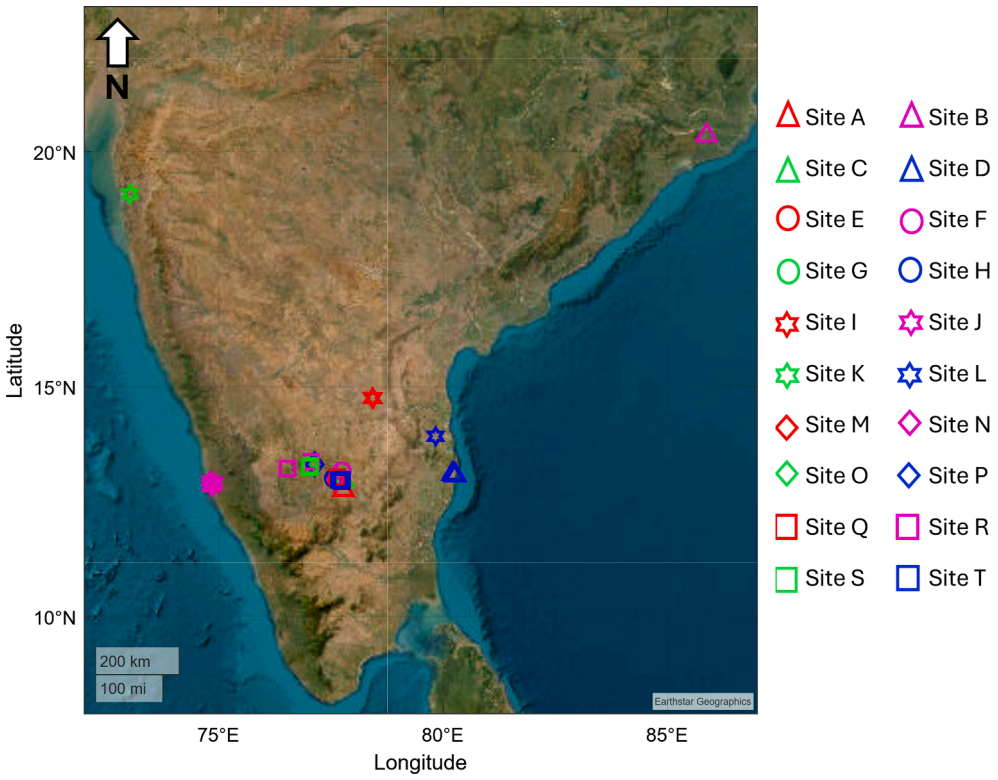

Fig. 4. Field SPT test locations used in this study. Site symbols represent different test conditions.

straightforward approach- the Force or Velocity Change Direction (FVCD) method, which offers improved accuracy while remaining feasible for real-world applications. The principles and validation of this method are explained in detail in the upcoming sections.

Despite the advancements in SPT analysis methods, challenges remain in accurately determining the ETR. The commonly used '2L/c' time window in the FV method has several limitations. Four major issues arise in the literature: the effect of short rod lengths, secondary impacts, the appropriate time window for ETR calculation, and the actual contribution of ETR to sampler penetration. The following sections address each of these four key issues in detail.

1.2. Short rod lengths and energy transfer in drill rod

The effect of short rod lengths (i.e., rod length less than 9 m, with significant effect observed below 6 m) on energy measurements has been widely debated. Short rods tend to result in unexpectedly high energy measurements, leading some researchers to suggest rod length corrections [11,14,15]. At a later stage, Sy and Campanella [12] recommended that no rod length correction be used for the FV method. Meanwhile, Morgano and Liang [15] highlighted that- total energy transfer is independent of rod length, the percentage of kinetic energy converted to stress wave energy decreases with shorter rods, falling to as low as 86 %. However, they did not explain the relationship between FV and rod length and incorrectly suggested increasing the blow count for lesser energy transfer when using short rods. They argued that no rod length correction is needed since sampler penetration is independent of rod length. However, more recent findings by Cetin et al. [16] suggest that rod length corrections are required for the cases where $L^*N < 13$ (where L is rod length in m, and N is SPT-N value). This ongoing discrepancy highlights that, although rod length correction is often considered unnecessary in the FV method, short rods still exhibit lower energy transfer, which remains unresolved.

Additionally, most studies focus on energy measurement at the anvil level, and a few have also examined energy at the sampler level to understand the effect of hammer energy on sampler penetration, particularly in cases involving short rod lengths. Notably, Odebrecht et al. [17], Lukiantchuki et al. [18], and Hong et al. [19] reported conflicting findings on the variability of energy between the sampler and anvil levels. Odebrecht et al. [20] observed that energy at the sampler level in low-resistance soils exceeded that at the anvil. This contradicts the theoretical expectation that energy should dissipate as it reaches the sampler. Lukiantchuki et al. [18] also found that sampler-level energy is more variable than anvil-level energy, but did not explain this discrepancy clearly. More recently, Hong et al. [19] emphasized the importance of measuring energy at the sampler level, demonstrating that it improves correlation with static resistance. However, their study of the number of field test cases was limited (33 SPT in 3 boreholes), the effects of rod length (particularly short rods) were not explored, and the time window used for sampler energy calculation was not mentioned. Despite these findings, the significance of energy measurements at the sampler level has not been extensively studied, and its importance remains underexplored in previous research. The relationship between sampler penetration, ETR, and rod length for varying N values has yet to be fully validated in field conditions.

1.3. Wave propagation challenges in the FV method

Wave propagation within the drill rods presents another challenge in accurately calculating ETR. The energy transferred to the drill rod and the penetration depth for each blow depends on the soil's stiffness (N value) and the rod length. However, current ETR calculation procedures often fail to account for these variables effectively. Studies such as Abou-Matar and Goble [13] attempted to analyse stress distribution within solid rods, though the real tests use hollow rods. Additionally, the geometry of the hammer and the presence of joints and impedance interfaces further complicate wave propagation. Abou-Matar [21] noted that changes in cross-section lead to reflected forces and velocities that disrupt stress-velocity proportionality. Furthermore, safety hammers, which have a minimal thickness above the impact point, contribute to

Table 1
SPT test details of this study.

Test Location	Total Borehole	Rod length (m)	Soil layer	Total SPT	Total Blows
Site A	5	≤ 10	Silty Clay	24	957
		> 10	Gravely Sand	10	656
Site B	1	≤ 10	Silty Clay	3	38
		> 10	Silty Clay	5	85
Site C	4	≤ 10	Clayey Sand	20	918
		> 10	Weathered Rock	5	250
Site D	5	≤ 10	Sandy Silt	10	319
		> 10	Sandy Silt	2	100
Site E	6	≤ 10	Clayey Silt	35	1205
		> 10	Weathered Rock	7	343
Site F	1	≤ 10	Sandy Silt	4	78
		> 10	Sandy Silt	8	190
Site G	5	≤ 10	Silty Clay	26	849
		> 10	Weathered Rock	3	114
Site H	15	≤ 10	Clayey Silt	44	1767
		> 10	Sandy Silt	59	3272
Site I	1	≤ 10	Weathered Rock	2	9
Site J	5	≤ 10	Clayey Silt	19	592
		> 10	Weathered Rock	2	100
Site K	3	≤ 10	Sandy Clay	8	273
Site L	3	≤ 10	Sandy Silt	10	624
		> 10	Sandy Gravel	12	802
Site M	4	≤ 10	Clayey Silt	23	245
		> 10	Sandy Silt	14	219
Site N	5	≤ 10	Sand	9	343
		> 10	Sand	2	106
Site O	9	≤ 10	Sandy Silt	37	1179
		> 10	Silty Sand	19	1365
Site P	7	≤ 10	Sandy Silt	21	629
Site Q	4	≤ 10	Silty Clay	12	374
		> 10	Silty Clay	11	704
Site R	2	≤ 10	Sandy Clay	7	159
Site S	2	≤ 10	Sandy Silt	10	290
		> 10	Gravel	3	266
Site T	2	≤ 10	Silty Clay	3	22
		> 10	Silty Clay	3	51
Grand Total	89			492	19,493

stress cancellations due to wave superposition, although this is inconsistent across all tests. Stress waves generated by the most commonly used hammer- automatic and donut-type tend to reflect at joints between rods and create complex interactions between transmitted and reflected waves. The force profile after the first peak indicates that the one-dimensional (1D) wave equation, often used for energy calculations, is inadequate for real-world scenarios. The complex wave reflections at each joint make pinpointing the tension cut-off time more difficult and also challenge accurate energy integration, as shown in Fig. 1. Schematic SPT test conditions, wave propagation, and respective energy integration for the anvil and sampler are shown in Fig. 1. It can be seen that the current energy estimation of integration up to '2L/c' adds up all reflected forces and velocities. Hence, this method becomes less accurate in real-world scenarios, where wave reflections are more complicated and unpredictable.

1.4. ETR time window Considerations and secondary impacts

The time window for ETR estimation is crucial in SPT hammer energy measurement. Traditionally, the FV method considers the time from the impact point to tension cutoff time, that is '2L/c' time window. Later, this window was extended to infinity, allowing for the consideration of secondary, tertiary, and subsequent hammer impacts on the anvil. However, each impact follows its own '2L/c' window until the stress waves cease [23,24]. Schmertmann and Palacios [11] observed that 90 % of energy transfers occur within the '2L/c' time window, after which energy no longer contributes to sampler penetration. Farrar [25] pointed out that shorter rod lengths limit the '2L/c' window, preventing full attenuation of the stress wave. Contrarily, Daniel et al. [26] found that ETR during secondary impacts occurs early enough to contribute to sampler penetration, especially in loose soils (N value < 30). They concluded that secondary impacts do not significantly affect short rod corrections and that the delayed ETR still contributes to sampler penetration. Additionally, secondary impacts play a critical role in ETR calculation [15]. Some studies argue that secondary impacts should not be included in energy measurements because they occur after the '2L/c' window and do not contribute to sampler penetration [11]. However, other studies suggest that secondary impacts occur within the '2L/c' window and should be considered in energy estimation [15]. There are also studies indicating that secondary impacts can occur both before and after the '2L/c' window, further complicating the consensus on whether they should be included in ETR calculations [22,26]. Cavalcante [27] found that secondary impacts contribute to sampler penetration and that their timing depends on soil stiffness and strength (N value), stressing that delayed energy is still effective. Despite these findings, there is no consensus on the optimal time window for energy estimation applicable across all ranges of N values and rod lengths. Additionally, there is no evidence of recorded video studies on sampler penetration.

1.5. Visual measurements in SPT

Researchers have explored visual measurement techniques during SPT testing to analyze the complex movements of the SPT drill rod assembly, including the hammer, anvil, and drill rod. Santana et al. [28] used a camera and a manually held measuring staff to estimate the vertical displacement of the anvil and hammer, as shown in Fig. 2(a). However, this approach was limited by the low resolution of the staff markings (5 mm least count) and the difficulty of manually holding the staff in vertical alignment. Lee et al. [29] introduced rectangular black-and-white markers (Fig. 2(b)) and a digital line-scan camera to track

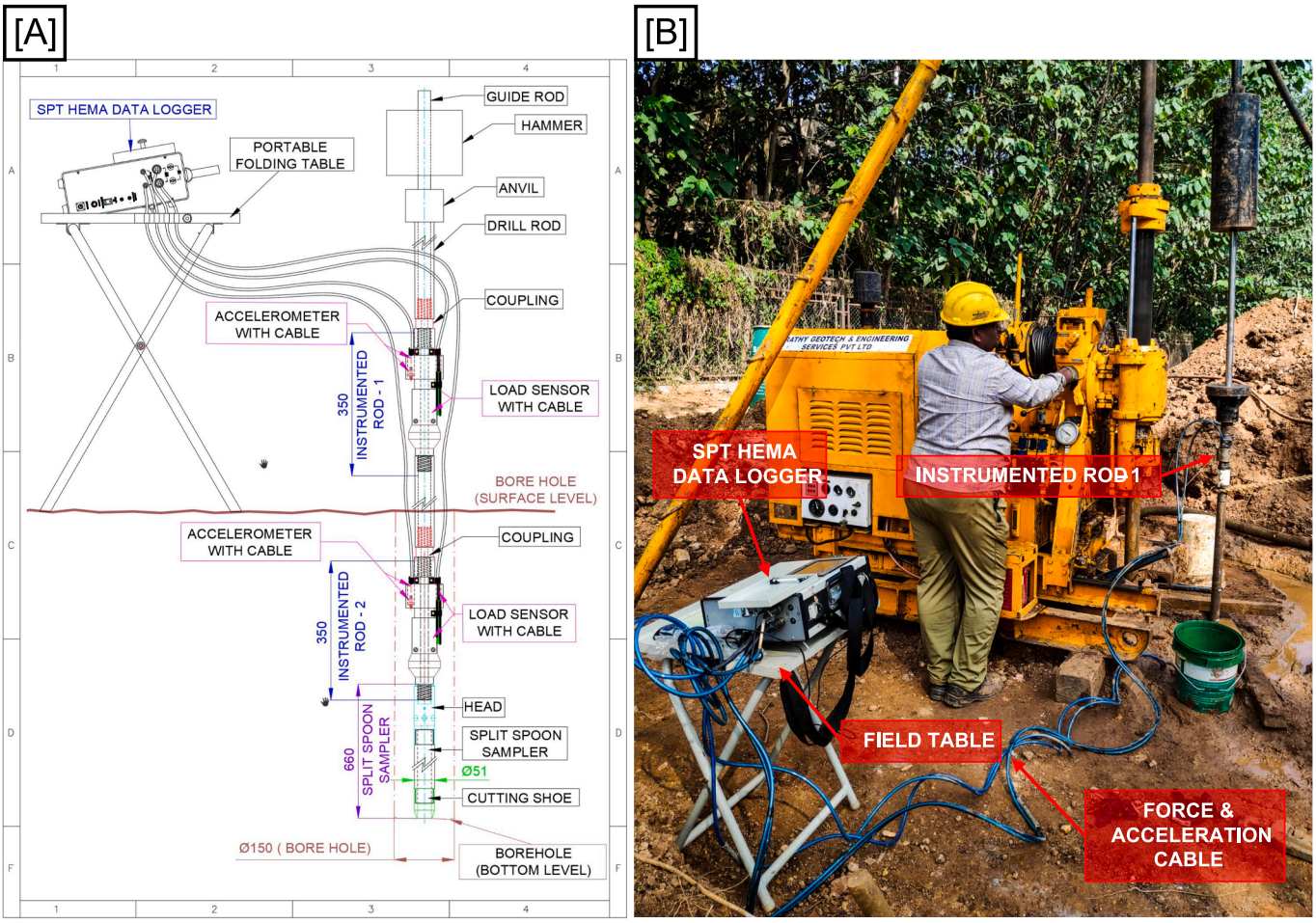

Fig. 5. SPT hammer energy measurement by SPT HEMA using two instrumented rods: [A] Schematic and [B] Field SPT setup.

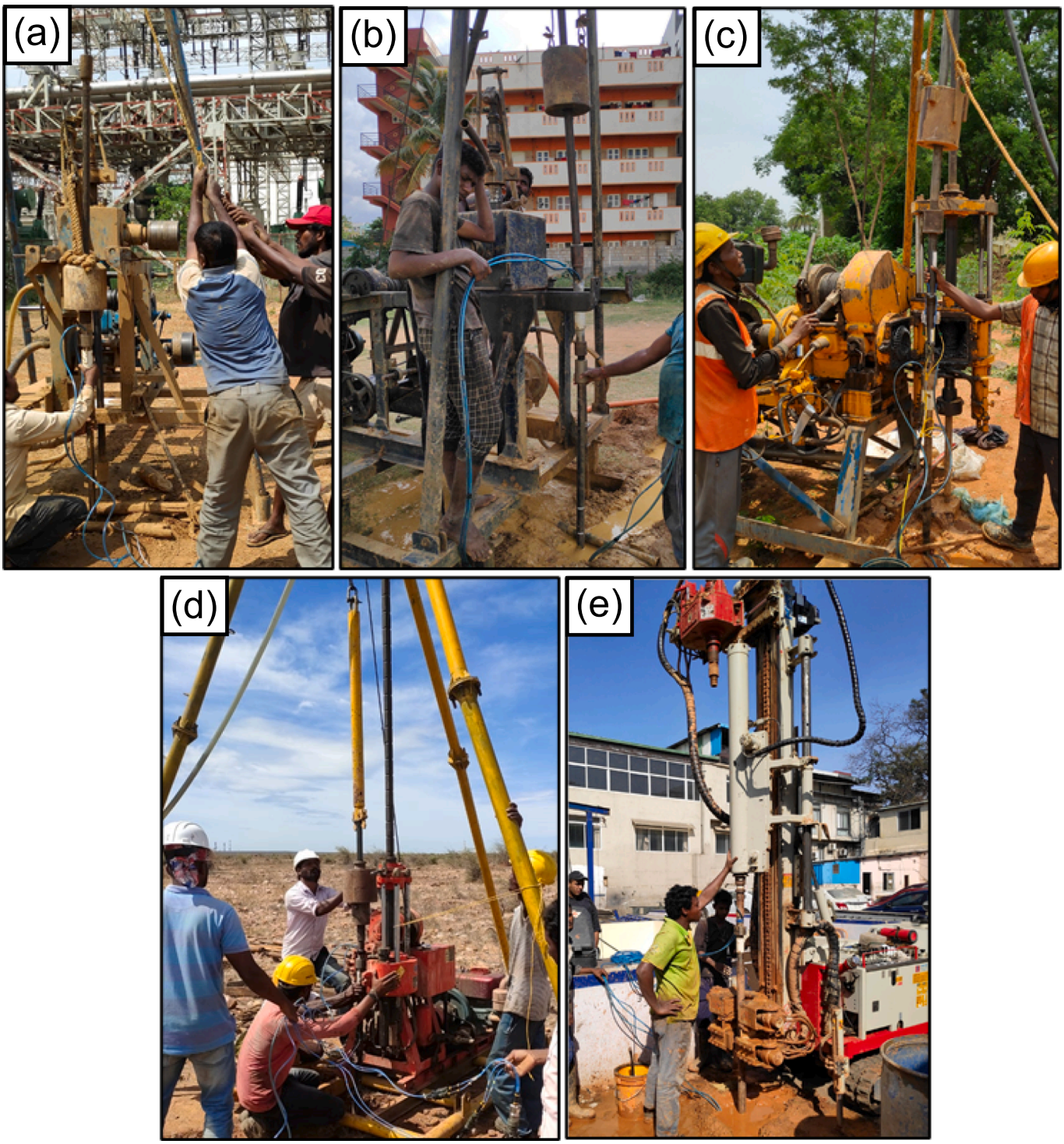

Fig. 6. Typical SPT hammer energy measurement at various sites using SPT HEMA with two instrumented rods across various rigs and hammer-dropping mechanism configurations:: (a) Rotary drill rig with rope and pulley for manual lifting hammer, (b) Rotary drill rig with spool winch for motorised lifting hammer, (c) Hydraulic drill rig with spool winch for motorised lifting hammer, (d) Hydraulic drill rig with Auto-trip hammer, and (e) Multipurpose drill rig with Automatic hammer.

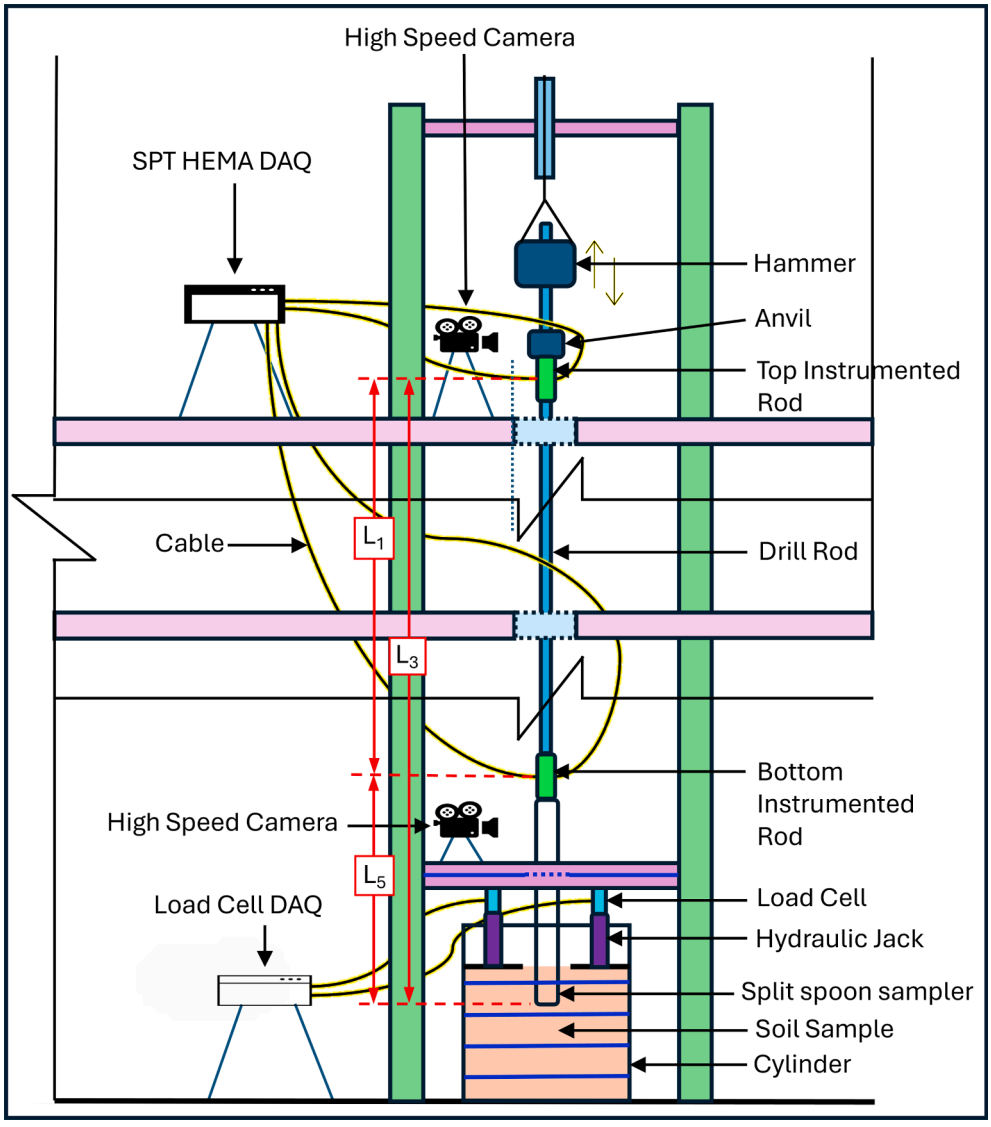

Fig. 7. A schematic sectional view of the SPT laboratory setup at IISc illustrates the detailed testing arrangement used for the study.

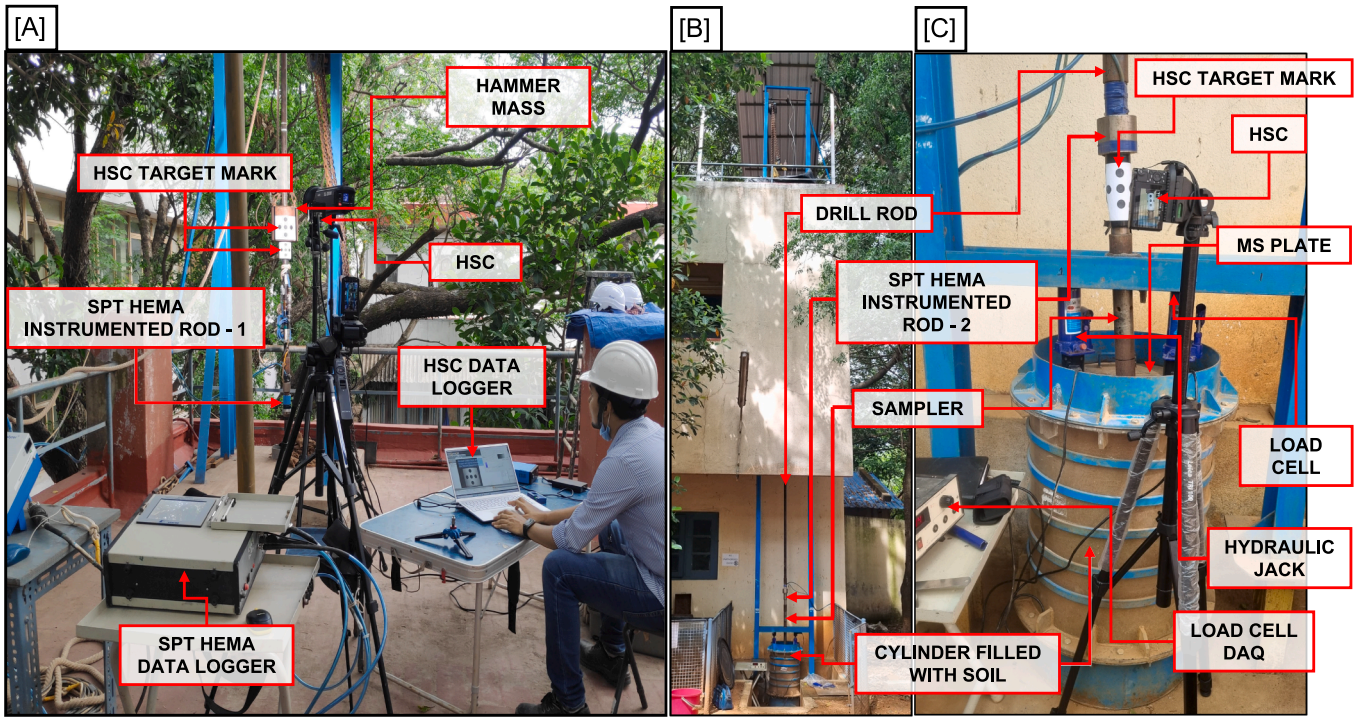

Fig. 8. Laboratory SPT model setup with two instrumented rods of SPT HEMA and HSC: [A] Testing arrangements at Roof Top, [B] Front view of the entire Laboratory setup building, and [C] Soil sample mould with instrumentation.

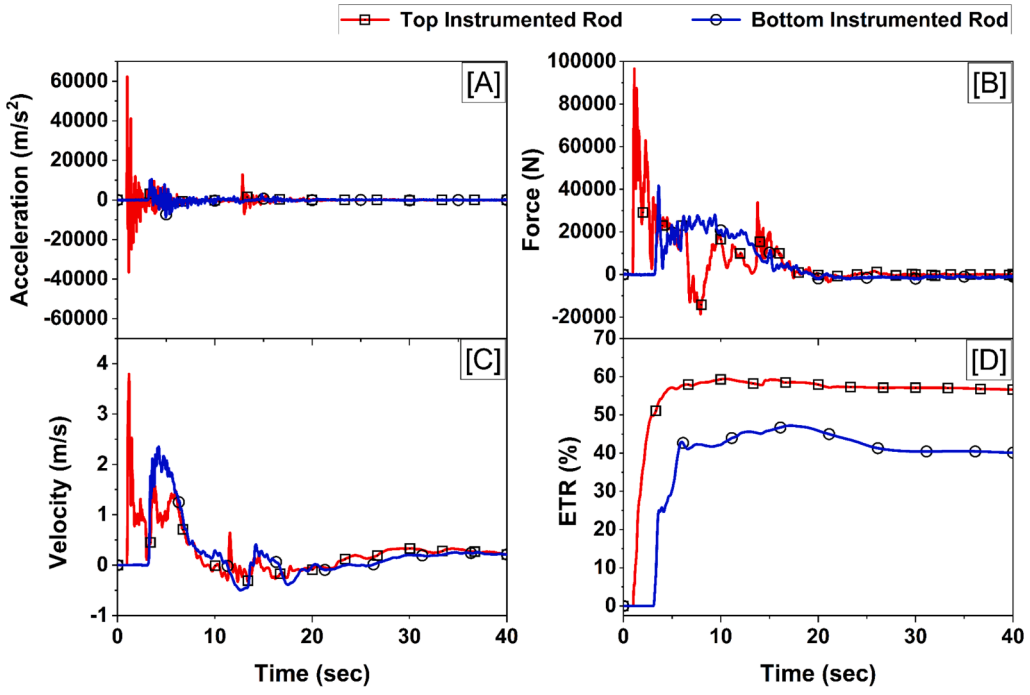

Fig. 9. Typical raw data plots from SPT HEMA Instrumented Rods at Anvil and Sampler levels: [A] acceleration, [B] force, [C] velocity, and [D] ETR.

hammer and anvil movements. This method focused on vertical movement to study secondary impacts on energy transfer and anvil penetration. Similarly, Lee et al. and Lim et al. [30,31] used triangular target markers and line scan cameras (Fig. 2(c)) in pile driving analysis. Building on this, Lee et al. [23,29] applied this marker and line scan camera for tracking hammer and anvil motion. However, these methods were restricted to the vertical movement of the SPT system. These markers provided data on marker width and line inclination, offering 2D displacement information, but encountered challenges on curved surfaces like the hammer, anvil, and drill rod. Image distortion reduced measurement accuracy, and maintaining a perpendicular camera view of the target picture was difficult. Line-scan cameras also had limitations, capturing only displacements in the viewing direction while missing multi-directional and rotational movements. Additionally, studies by Lim et al. and Lee et al. [23,29,31] lacked field test photographic documentation, restricting validation and replication. These

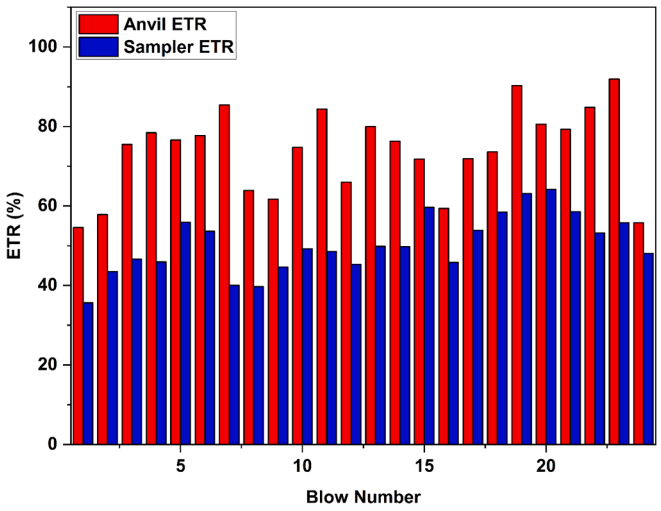

Fig. 10. Typical ETR from Anvil and Sampler level Instrumented Rods of SPT HEMA for an SPT-N value of 24.

challenges highlight the need for a more comprehensive approach to capturing full-range SPT component movements during field testing.

To overcome the above limitations of these previous methods, Yadhunandan and Anbazhagan [32] introduced High-Speed Camera (HSC) system with Circular target marks (shown in Fig. 2(d)) to measure the movements of the hammer, anvil, and sampler in all three dimensions (x, y, and z). In this study, HSC with circular target mark, hereafter called HSCCT, is engaged to study the rod displacement at both anvil and sampler levels during SPT.

The insights and limitations discussed across the above subsections highlight the need for a more practical and accurate method for energy estimation in SPT. This study addresses unresolved issues related to energy discrepancies in short rod cases, wave propagation challenges in the FV method, and, most importantly, identifying an optimal time window to overcome these existing limitations in ETR calculation in SPT. It aims to overcome the limitations of previous research by investigating alternative dynamic time windows for ETR calculation using force and acceleration data. In a controlled laboratory full-scale SPT model setup, HSCCT recordings were employed to capture precise movements of the drill rod assembly during energy measurements at both the anvil and sampler levels. Displacements were estimated for

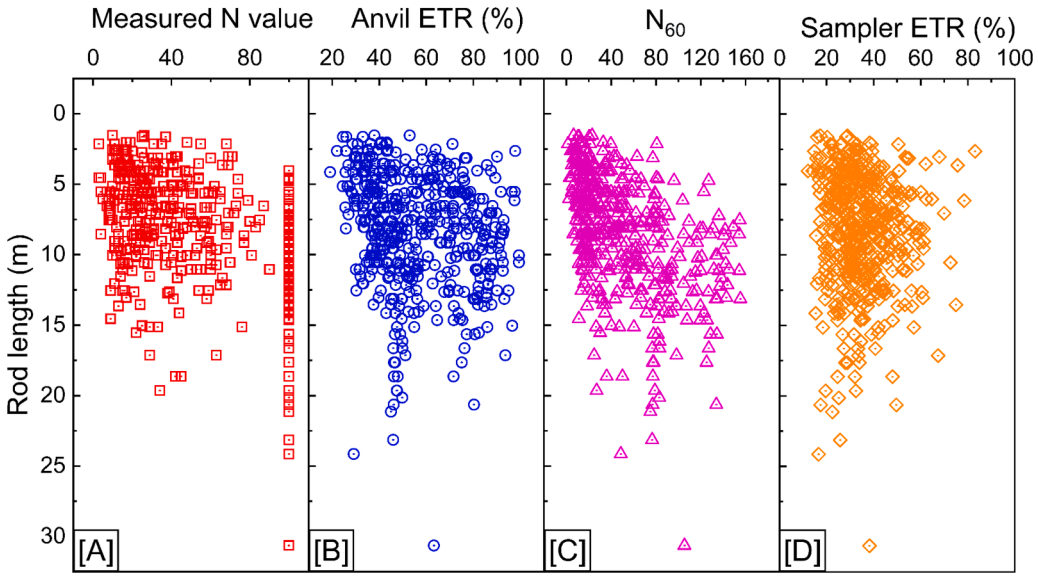

Fig. 11. Distribution of field SPT datasets with Rod length: [A] measured N value, [B] Anvil ETR, [C] N60, and [D] Sampler ETR.

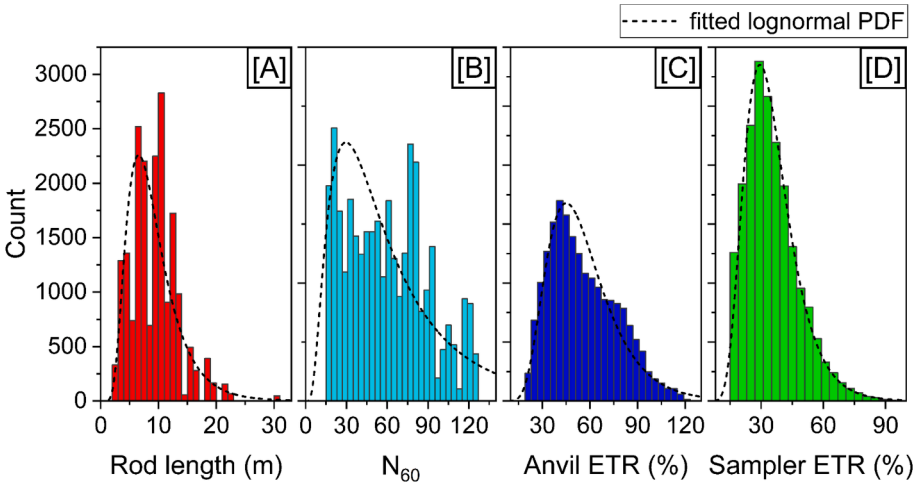

Fig. 12. Histograms with fitted lognormal PDF for field SPT datasets: [A] Rod length, [B] N60, [C] Anvil ETR, and [D] Sampler ETR.

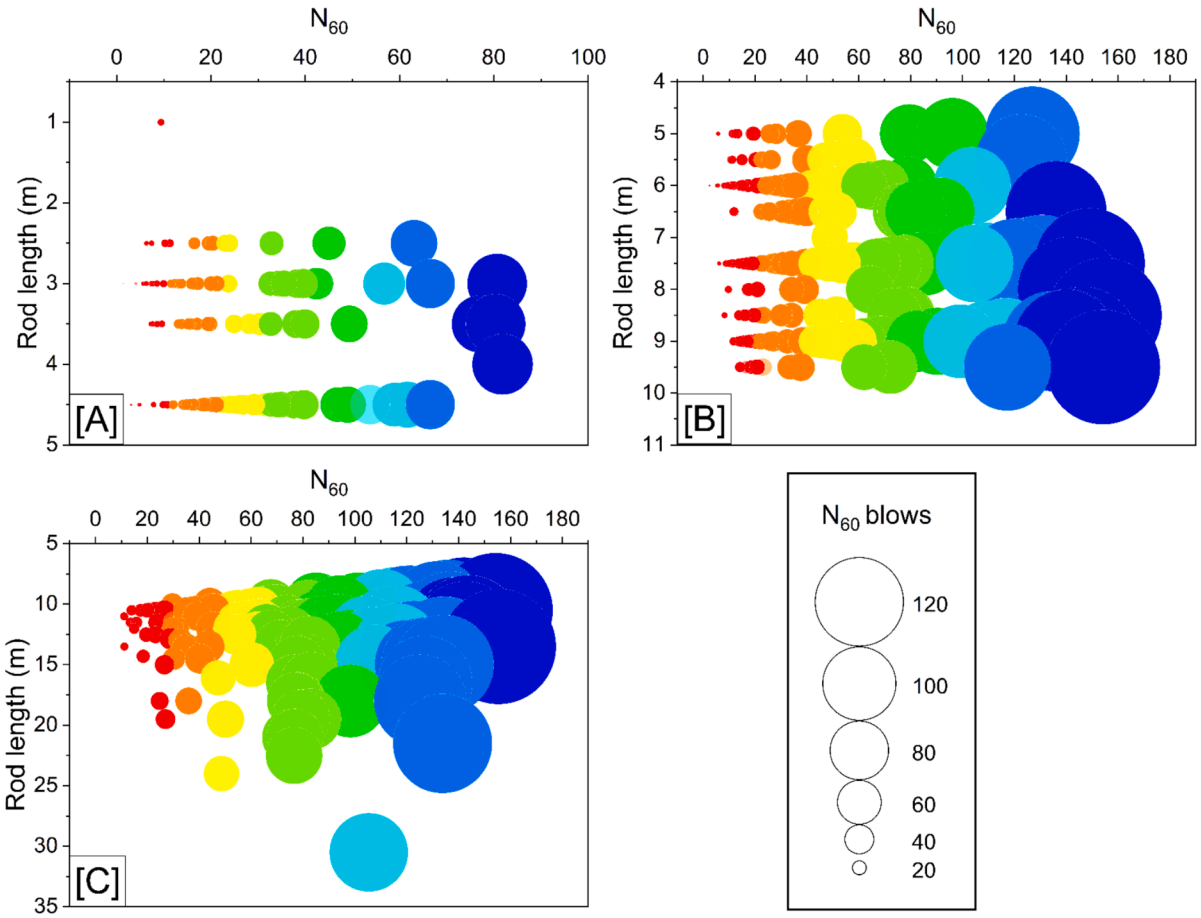

Fig. 13. Distribution of N60 values concerning Rod length: [A] Rod lengths less than 5 m, [B] Rod lengths 5 to 10 m, and [C] Rod lengths greater than 10 m.

each test using the HSCCT data. Based on this combined instrumentation and visual data, a new method- FVCD, is introduced to determine a more accurate and dynamic time window for ETR estimation. This method improves the accuracy of hammer energy estimation by dynamically identifying the cutoff point based on waveform behaviour. It is validated using 492 field and 44 laboratory SPTs (20,000 + hammer blows) and can serve as a reliable alternative to the conventional FV method, particularly for short rods and variable site conditions. The main contribution of this study is the introduction and validation of the FVCD method, which provides a more accurate and practical way to estimate hammer energy for different rig types, rod lengths, soil conditions, and N values.

2. Methodology and experiments

2.1. Methodology

The study aims to provide a reliable SPT hammer energy estimation regardless of rig types, rod lengths, soil conditions, and N values. Therefore, both laboratory and field testing are necessary, with provisions to measure energy across various rod lengths, soil conditions, and N values. A SPT energy measurement setup called SPT HEMA (SPT Hammer Energy Measurement Apparatus), capable of measuring force and acceleration simultaneously at both the anvil and split-spoon sampler levels, is used in a full-scale SPT laboratory model setup along with extensive field experiments. Further, to validate the sensor-based energy measurements from SPT HEMA, a non-contact visual measurement method using HSCCT recordings is also employed. Detailed waveform observations from both sensor-based and visual-based measurements, including force, velocity, displacement, and ETR, were analyzed across various soil stiffness conditions (N values) at both anvil and sampler levels. In addition, the FVCD method was compared against the conventional FV method using a large dataset, and the results were supported with detailed statistical analysis. The step-by-step procedure followed throughout the study is illustrated in Fig. 3, which shows the methodology flowchart including laboratory and field SPT testing, ETR calculation using FV and FVCD methods, validation using visual measurement data, and final comparison and interpretation. The FVCD method, explained in detail in *Section 3.2.2*, is included in the flowchart to provide an early overview of the complete methodology.

2.2. Field SPT setup and experiments

This study investigates the impact of individual hammer blows on ETR measurement in SPT conducted in both field and laboratory SPT setups. In the field, 492 SPT tests were conducted across 89 boreholes drilled in various geological formations within the Indian peninsular region. Fig. 4 presents a location map indicating the borehole placements at each test site, designated as Site A to Site T (a total of 20 test sites). The test sites are strategically chosen across the peninsular region of India, comprising Bangalore, Chennai, Thumakur, Mangalore, Mumbai, Bhubaneshwar, and YSR Kadapa. These locations exhibit diverse soil subsurface features, reflecting the geological background of the Deccan plateau formations and influences from crystalline and metamorphic rocks. Black and Laterite soils are dominant soil types in parts of southern India and were potentially encountered during the SPT tests conducted in Chennai and Mangalore. The depths explored during the SPT tests ranged from 0.5 m to 30 m, encountering a variety of soil types such as clay, sand, and mixtures of silt and gravel, with varying groundwater levels. A total of 19,493 SPT hammer blows were recorded,

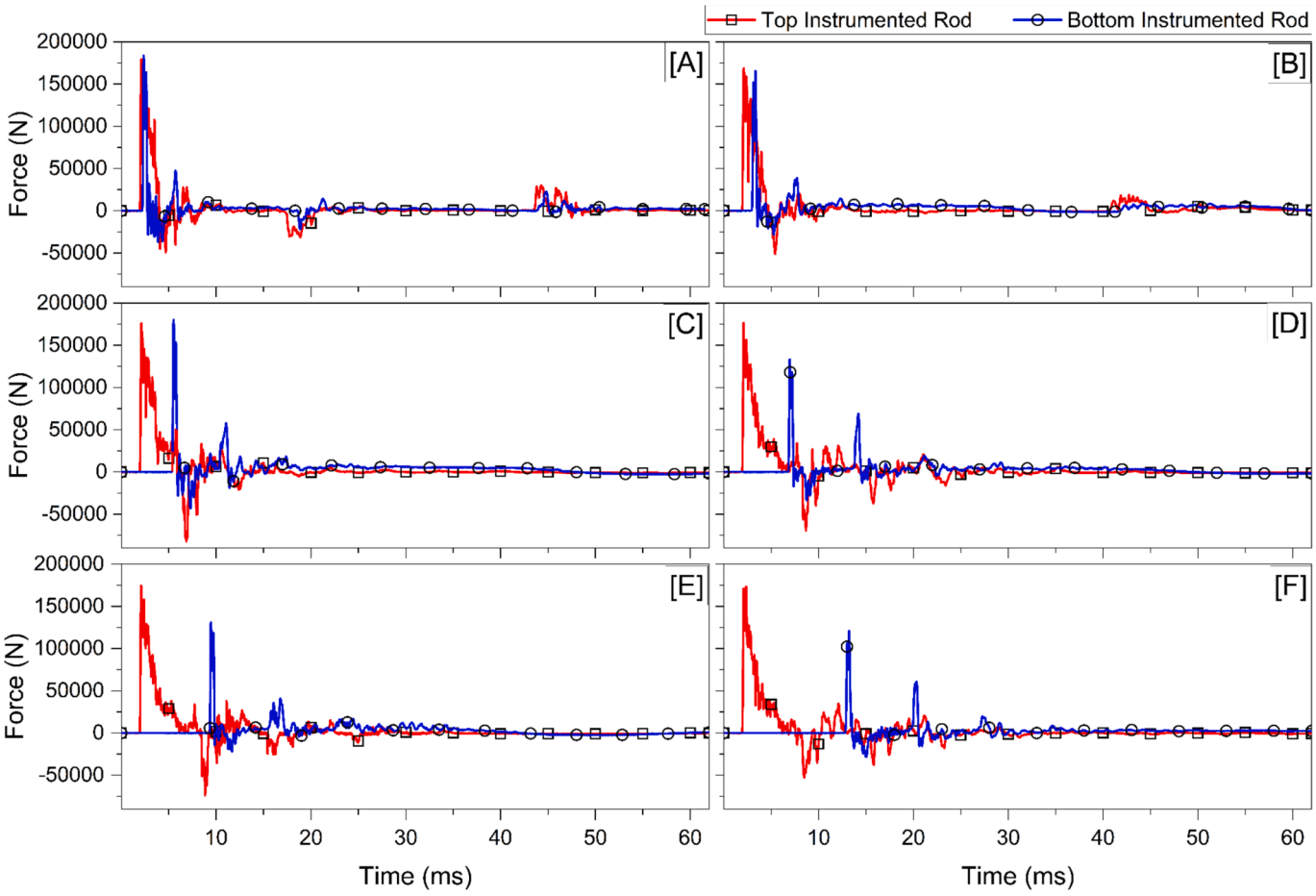

Fig. 14. Typical time history force of top and bottom instrumented rod for rod lengths [A] 1 m, [B] 5 m, [C] 10 m, [D] 15 m, [E] 20 m, and [F] 30 m.

providing a comprehensive dataset for analyzing the influence of individual blows on ETR. Table 1 summarises the details of the SPT tests performed at each test site.

The current study utilises the SPT HEMA illustrates both the schematic and field setup in Fig. 5. Each test employed two instrumented rods- one just below the anvil (also called the top instrumented rod or top sensor) and the other just above the sampler (also called the bottom instrumented rod or bottom sensor). This configuration allows for the measurement of ETR at both the anvil level (Anvil ETR) and the sampler level (Sampler ETR). The experiments cover various SPT rigs and hammer-dropping mechanisms commonly engaged in most countries. These included rotary, hydraulic, and automatic drill rigs. Similarly, the hammer-dropping mechanisms employed multiple methods, such as manual rope and pulley systems, dropping through a cathead, trip mechanisms, and automatic hammers. Fig. 6 shows the typical SPT HEMA system recording hammer efficiency using two instrumented rods across various rigs and hammer-dropping mechanism configurations.

2.3. Laboratory SPT setup and experiments

A controlled full-scale laboratory SPT model setup was built at the existing building of the soil mechanics laboratory, civil engineering department, at IISc Bangalore. To facilitate SPT testing, 150 mm diameter holes were cut into the floor slab, allowing the tests at various levels to simulate varying drill rod lengths and test depths. Fig. 7 shows a schematic sectional view of the SPT laboratory setup at IISc and the detailed testing arrangement used. Fig. 8 provides a multi-perspective view of the laboratory SPT model setup. This includes an overhead layout, a close-up of the SPT instrumentation, and an overall front elevation view of the laboratory building. A soil cylinder filled with a sand sample is used for the test. The test has the provision to apply overburden pressure on the soil sample to simulate the field condition. Two instrumented rods were used to record acceleration up to 10,000 g and load up to 240 kN. Data acquisition was performed at a 60 kHz sample rate per channel. SPT hammer impact, anvil, sampler, and drill rod movement were recorded using HSC (Pco 1200hs, Sony DSC-RX100M5A) with the circular target markings at 1087 and 1000 fps (frames per second). The collected data were processed using the MATLAB program for filtering, signal conditioning, and motion tracking. Further details on the setup, methodology, and data processing are provided by Yadhunandan and Anbazhagan [32].

3. Results and Discussion

3.1. Field data acquisition and results

In the field, SPT hammer energy is measured for all the boreholes and all the test depths at both the anvil and sampler levels. All waveforms of hammer impact during SPT are measured using SPT HEMA. Fig. 9 shows typical time history plots of the raw data obtained from a single SPT hammer blow in these field SPT setups. The instrumentation records the force and acceleration data; the velocity data is derived by integrating the acceleration data and considering up to '2L/c' tension cut-off time as per the FV method, and ETR is calculated. Fig. 10 shows the ETR comparison from the top and bottom instrumented rods of a typical SPT-N value of 24. This comparison helps to assess how efficiently the hammer energy is transferred down the drill rods and ultimately reaches the soil sampler. The results show that the Anvil ETR is consistently

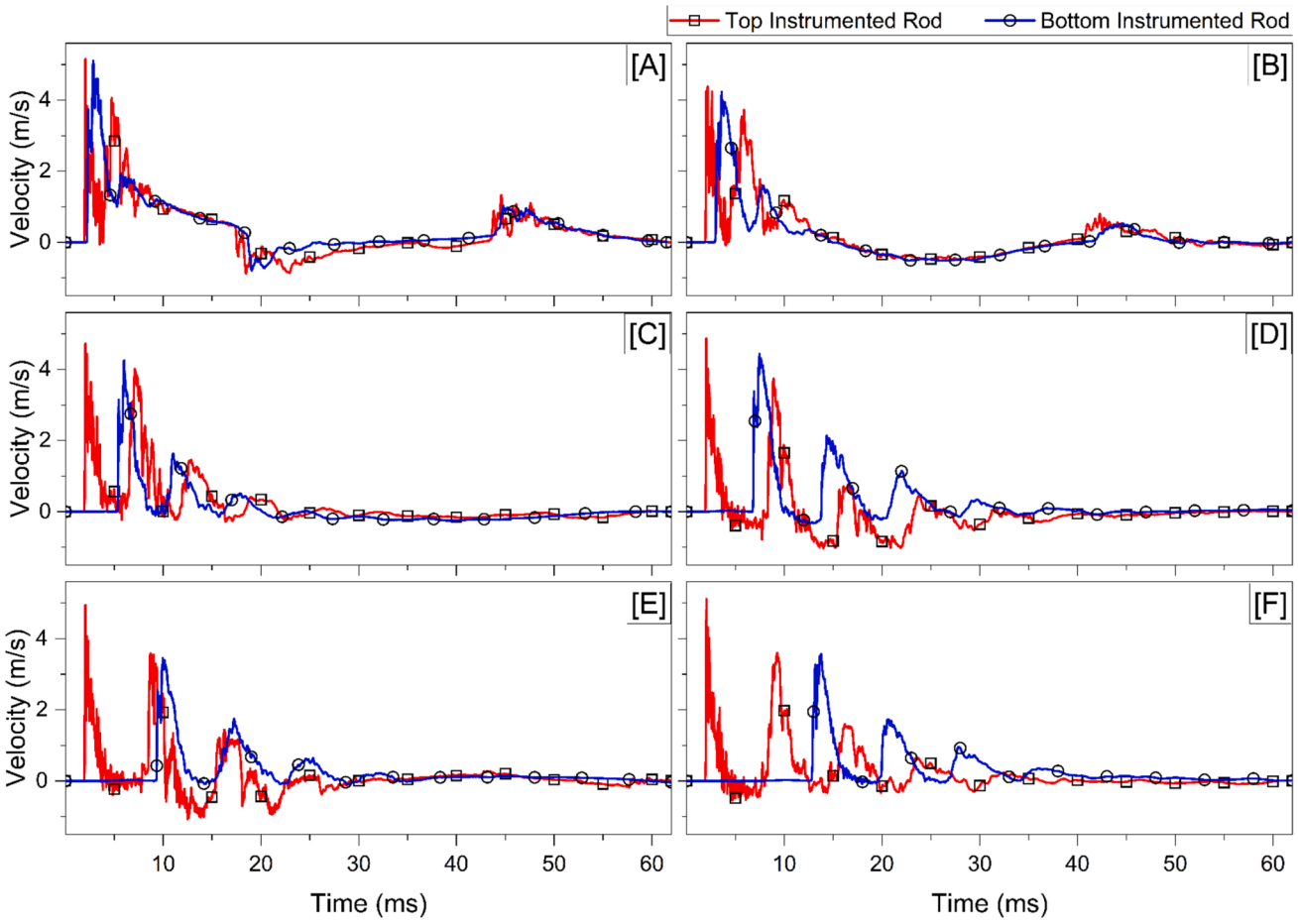

Fig. 15. Typical time history velocity of top and bottom instrumented rod for rod lengths [A] 1 m, [B] 5 m, [C] 10 m, [D] 15 m, [E] 20 m, and [F] 30 m.

higher than the Sampler ETR. This indicates energy loss along the drill rod. Additionally, ETR varies with each blow, highlighting the necessity of measuring ETR for all blows at every SPT test depth. Fig. 11 shows the distribution of field SPT data sets of measured N value, Anvil ETR, N_{60}, and Sampler ETR with Rod length. Fig. 12 shows a histogram of field SPT datasets for four key random variables: rod length, N_{60}, Anvil ETR, and Samper ETR. These variables naturally vary across different test conditions; hence, they were treated as random in this study. Rod length varies based on test depth, N_{60} varies with soil resistance, Anvil ETR varies due to hammer energy transfer efficiency, and Sampler ETR depends on rod length, number of joints, and energy losses. The overlaid dashed curves represent lognormal probability density function (PDF) fits, which help visualize the underlying distribution patterns. The data distribution and histogram show a wide range of values, which indicates variability in ETR and penetration resistance across various rod lengths. This distribution and histogram confirm a sufficient dataset for further analysis and interpretation.

Fig. 13 presents bubble charts illustrating the distribution of N_{60} values, representing the number of blows, against various ranges of rod length intervals. The bubble graphs visually represent how the frequency of specific N_{60} values varies with rod length and the bubble size corresponding to the frequency of repeated values. For example, smaller N_{60} values (less than 20) appear mostly between rod lengths of about 2.5 m and 12 m. Beyond this depth, very few or no N_{60} (less than 20) values are observed, which means that deeper layers usually don't show such low resistance. Further looking at the three depth ranges (< 5, 5–10, and > 10 m) more broadly, rod lengths under 5 m generally have smaller N_{60} values, indicating that shallow depth often corresponds to fewer blows, suggesting a looser material, and higher resistance values are uncommon. For rod lengths between 5 and 10 m, a broader range of N_{60} values is observed, with varying frequencies. It indicates varying soil conditions, from loose to moderately compacted material. For rod lengths greater than 10 m, the distribution shifts noticeably toward higher N_{60} values. It indicates deeper depths frequently encounter denser or more compact strata. This bubble chart representation helps visualize the data's overall distribution and frequency more clearly than using only distribution scatter plots or histograms.

Figs. 14-16 illustrate the typical force, velocity, and ETR time history data of top and bottom instrumented rods for rod lengths of [A] 1 m, [B] 5 m, [C] 10 m, [D] 15 m, [E] 20 m, and [F] 30 m. These results are derived from one of the boreholes at Site F, chosen due to the consistent soil layers (Sandy Silt) present at the test site. An automatic rig and automatic hammer setup were employed for the tests, ensuring minimal variation in the hammer blows for each strike and reducing errors in the setup compared to other types of hammer-dropping mechanisms and SPT rigs. The blows were randomly selected from the N value, generating typical plots. Analysing the relationship between rod length, N value, and ETR from field data proved challenging, and definitive conclusions could not be made. This difficulty arises because the test control below the ground inside the borehole cannot be observed from the ground level. Additionally, variations in SPT test procedures, component types, hammer drop mechanisms, and other field conditions, as shown in Fig. 6, create significant inconsistencies in the results. Even with standard equipment like automatic SPT setups, the depth of the SPT test and the corresponding soil layer stiffness vary. While maintaining the rod's verticality above ground is manageable in field tests, it cannot be observed or controlled inside the borehole. The SPT component's movements above the ground for various SPT rigs are analysed using

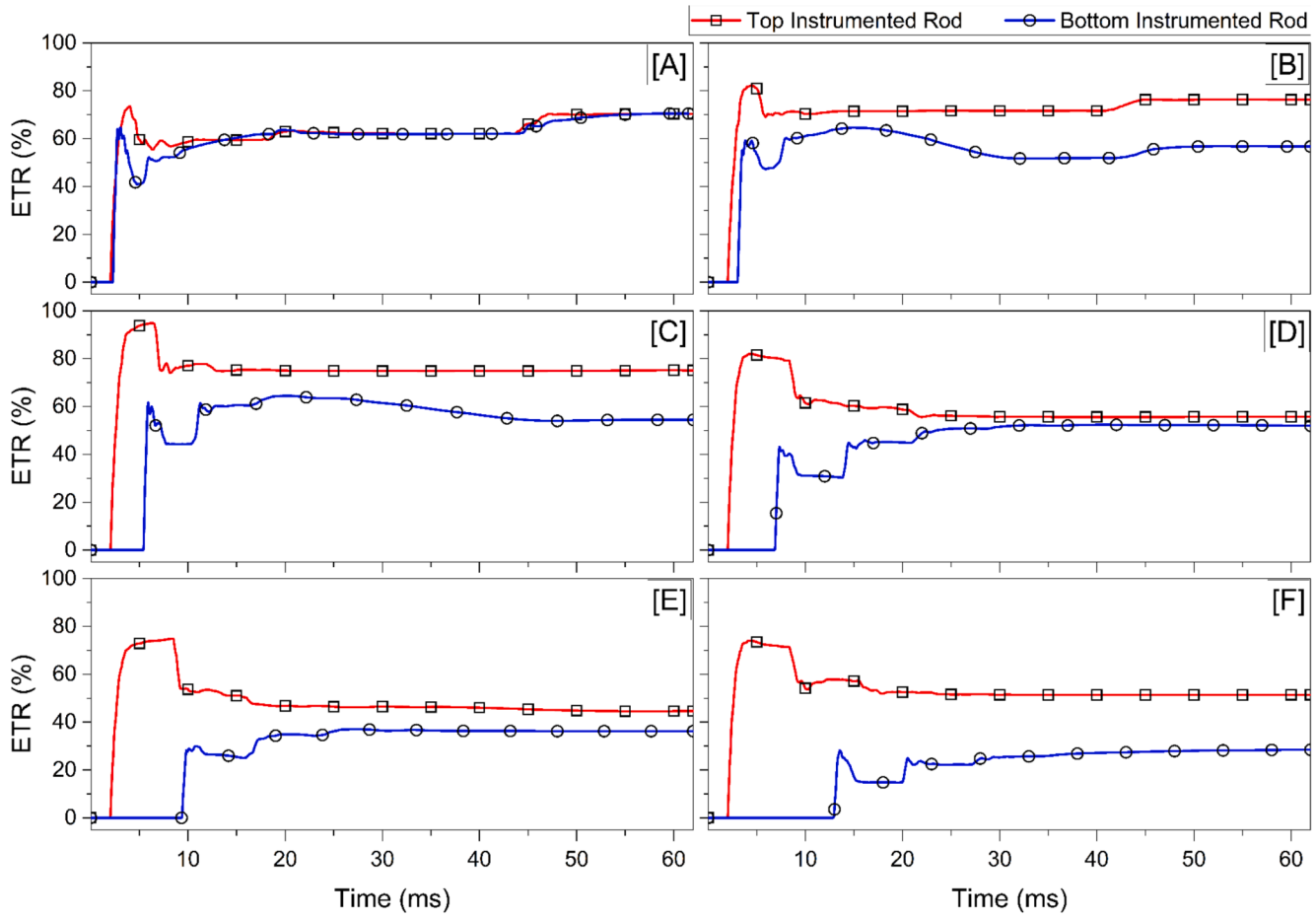

Fig. 16. Typical time history ETR of top and bottom instrumented rod for rod lengths [A] 1 m, [B] 5 m, [C] 10 m, [D] 15 m, [E] 20 m, and [F] 30 m.

Table 2
Description of significant time durations (t_1 to t_8) for waveform and energy transfer analysis.

Time	Description
t_1	Represents the 'L_1/c' stress wave travel time from the top sensor's measurement point (at anvil level) to the bottom sensor's measurement point (at sampler level), where L_1 is 8.36 m (L_1 is as shown in Fig. 17), and corresponding t1 is 2.63 ms
t_2	Represents the arrival time of the stress wave at the bottom sensor from the top sensor (which is theoretically equal to t_1)
t_3	Represents the '$2L_3/c$' stress wave travel time from the top sensor's measurement point (tension cutoff time of top sensor), where L_3 is 9.19 m (L_3 is as shown in Fig. 17), and the corresponding t_3 is 4.59 ms
t_4	Represents the time for either the force or velocity to first change its direction from positive to negative for the top sensor (at the anvil level) after the hammer blow
t_5	Represents the '$2L_5/c$' stress wave travel time for the bottom sensor (tension cutoff time of bottom sensor), where L_5 is 0.985 m (L_5 is as shown in Fig. 17), and the corresponding t_5 is 3.385 ms
t_6	Represents the time for either the force or velocity to first change its direction from positive to negative for the bottom sensor (at the sampler level) after the hammer blow
t_7	Represents the time for accumulating peak anvil vertical displacement measured from HSCCT
t_8	Represents the time for accumulating peak sampler vertical displacement measured from HSCCT

visual measurement and discussed by Yadhunandan and Anbazhagan [32]. Additionally, researchers [22] have noted that SPT drill rods can loosen after several blows, causing the drill rod assembly to buckle and leading to increased energy losses, which have not yet been studied. This is qualitatively evidenced by Fig. 16, showing that ETR reduces as rod length increases. Additionally, the penetration of the drill rod can be measured using an HSCCT with target markings and other visual measurement techniques at the anvil level, but it is impossible to measure at the sampler level inside a borehole. Therefore, understanding or concluding wave propagation results in SPT drill rods during field tests is challenging. Considering these variabilities, a controlled laboratory SPT model setup was used to study energy transfer efficiency during SPT hammer blows and sampler penetration in a controlled environment. The conclusions drawn from the SPT laboratory model tests are applied to field SPT test results to understand the significance of variations and to obtain improved and reliable test results. The results of field studies are explained in the subsequent sections.

3.2. Controlled laboratory experiments and their analysis

3.2.1. Analysis of ETR duration for various N values

In the laboratory SPT model tests, the soil sample densities are varied to achieve N values close to 5, 10, 20, 30, 50, and rebound (> 100). This allowed approximate penetration depths per blow of 60, 30, 15, 10, 6, and 3 mm, respectively. The ETR was maintained at around 60 % to ensure test uniformity. Random blows within the N value ranges are considered for the comparison and analysis of recorded data. Although all tests were conducted with rod lengths of 9.19 m (from the top sensor's measurement point to the bottom of the sampler – L_3, as shown in Fig. 7 and Fig. 17), they were sufficient to represent the long rod case to transfer energy, considering tension cutoff [26]. The instrumented rod just above the sampler is called the 'short rod' case. The rod length below the bottom instrumented rod (from the bottom sensor's measurement point to the bottom of the sampler – L_5, as shown in Fig. 7 and

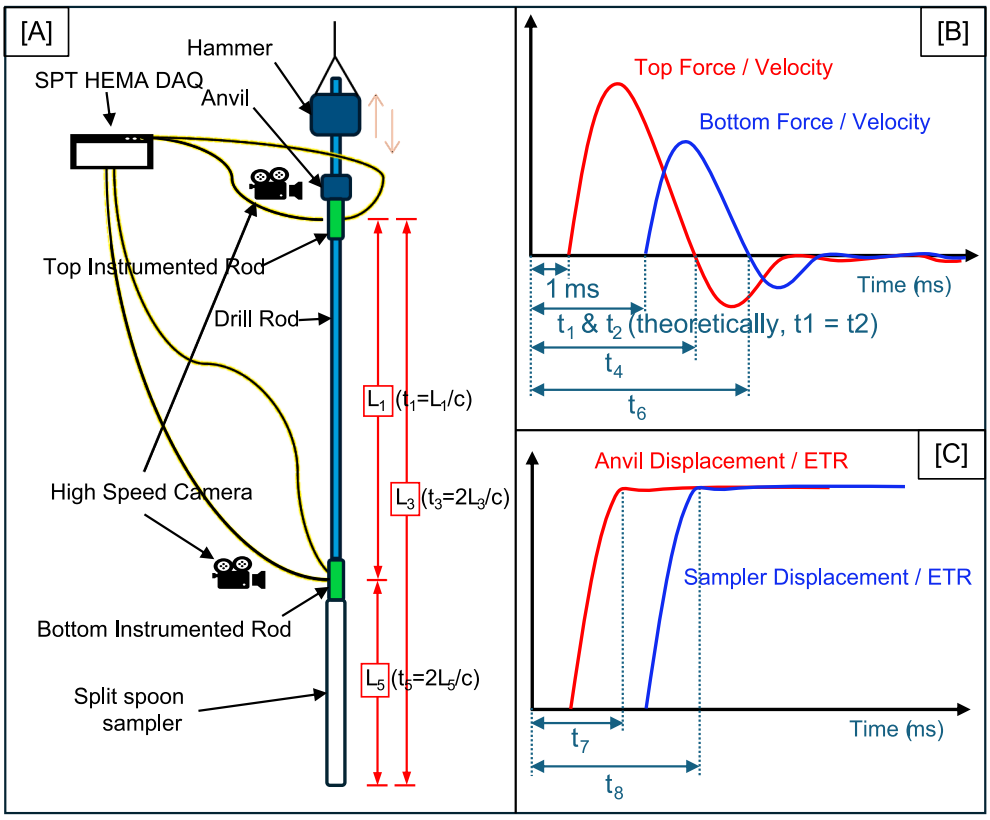

Fig. 17. Graphical representation of significant time durations (t_1 to t_8) for waveform and Energy transfer analysis in SPT- [A] Schematic of the SPT Drill Rod Assembly, [B] Force or Velocity Time History of the Top and Bottom Instrumented Rods, and [C] Displacement or ETR Time History of the Top and Bottom Instrumented Rods.

Fig. 17) measures 0.985 m. The study investigates how short and long rods perform for various N values, aiming to establish an energy estimation method applicable to all N values and rod length cases. To achieve this, the data plot showing the time history of the force, velocity, and ETR for the anvil and sampler level for various N values is used, as shown in Figs. 18-23. In these figures, plot [A] shows the force time histories at the anvil and sampler level; plot [B] shows the time history of force, velocity and displacement at the anvil level; plot [C] shows ETR at the anvil and sampler level; and plot [D] shows the time history of force, velocity and displacement at the sampler level. Further, in plots [B] and [D], the velocity is scaled graphically with respect to force to make the amplitude of force and velocity equal for visual purposes without changing numerical values. Additionally, these figures (Figs. 18-23) highlight eight significant time duration notations (denoted as t_1 to t_8) to analyze and compare waveform and energy transfer behaviours. The descriptions of the significant time durations are given in Table 2. All time durations are measured from the start of the waveform, which is defined as the zero line. The actual blow, or the initiation of the waveform, occurs at 1 ms, meaning a pre-trigger of 1 ms is considered before the start of the blow. These time durations are first illustrated graphically in Fig. 17 through – [A] Schematic of the SPT Drill Rod Assembly; [B] Force or Velocity Time History of the Top and Bottom Instrumented Rods; and [C] Displacement or ETR Time History of the Top and Bottom Instrumented Rods.

The analysis of the eight significant time durations for the laboratory data across various N-values is presented below. When analysing the times t_1 and t_2 in the plot [A] of Figs. 18-23, it can be seen that there is a time lag for the stress wave's arrival time at the sampler level from the anvil level (t_2) compared to the theoretical arrival time (t_1) as expected by Miller [33]. This delay suggests that the stress wave reaches the sampler later than expected in the real-world scenario. Several factors contribute to this phenomenon, including drill rod material properties, joint stiffness, and bonding between drill rods, etc. Additionally, we can extend this concept to the '2L/c' time, which corresponds to the arrival of the reflected wave at the anvil level after it travels from the top to the bottom of the drill rod assembly and reflects back. Abou Matar and Goble [13] found that the late arrival of reflected waves is probably due to loose connections in the drill string. Upon the arrival of the tensile wave back to the measurement point, force and velocity waveforms typically move in opposite directions. These plots reveal the challenge of visually identifying the reflected tensile wave's arrival point. When using a bottom sensor for measurements in a short rod scenario, the rod length below the sensor is minimal, resulting in a significantly lesser '2L/c' time. This short duration will not be sufficient to consider the accumulation of ETR with respect to time. The plot [C] of Figs. 18-23 clearly illustrates that t_5 is very short and the corresponding ETR is very low. Consider a scenario where the rod length is extremely small (close to zero meters); in such cases, the time window of '2L/c' is very small, and the ETR obtained after a blow may be negligible or even close to zero. Consequently, it can be concluded that limiting ETR consideration to the '2L/c' time window is inadequate, and energy transfer effects can extend beyond this boundary. Interestingly, energy transfer continues even after t_3 and t_5 for the anvil and sampler levels, respectively. However, most previous studies [17,18,19] that reported energy measured at the bottom sensor did not clearly explain how the energy was calculated or whether a 2L/c time window was used. Moreover, the appropriate time window that should be considered for all types of N values for long and short rod cases has not been specified or validated in any of the previous studies.

3.2.2. *Principle, Implementation, and validation of FVCD method*

To overcome the limitations of the fixed '2L/c' time window used in the conventional FV method, this study proposes a new approach called the Force or Velocity Change Direction (FVCD) method. This method

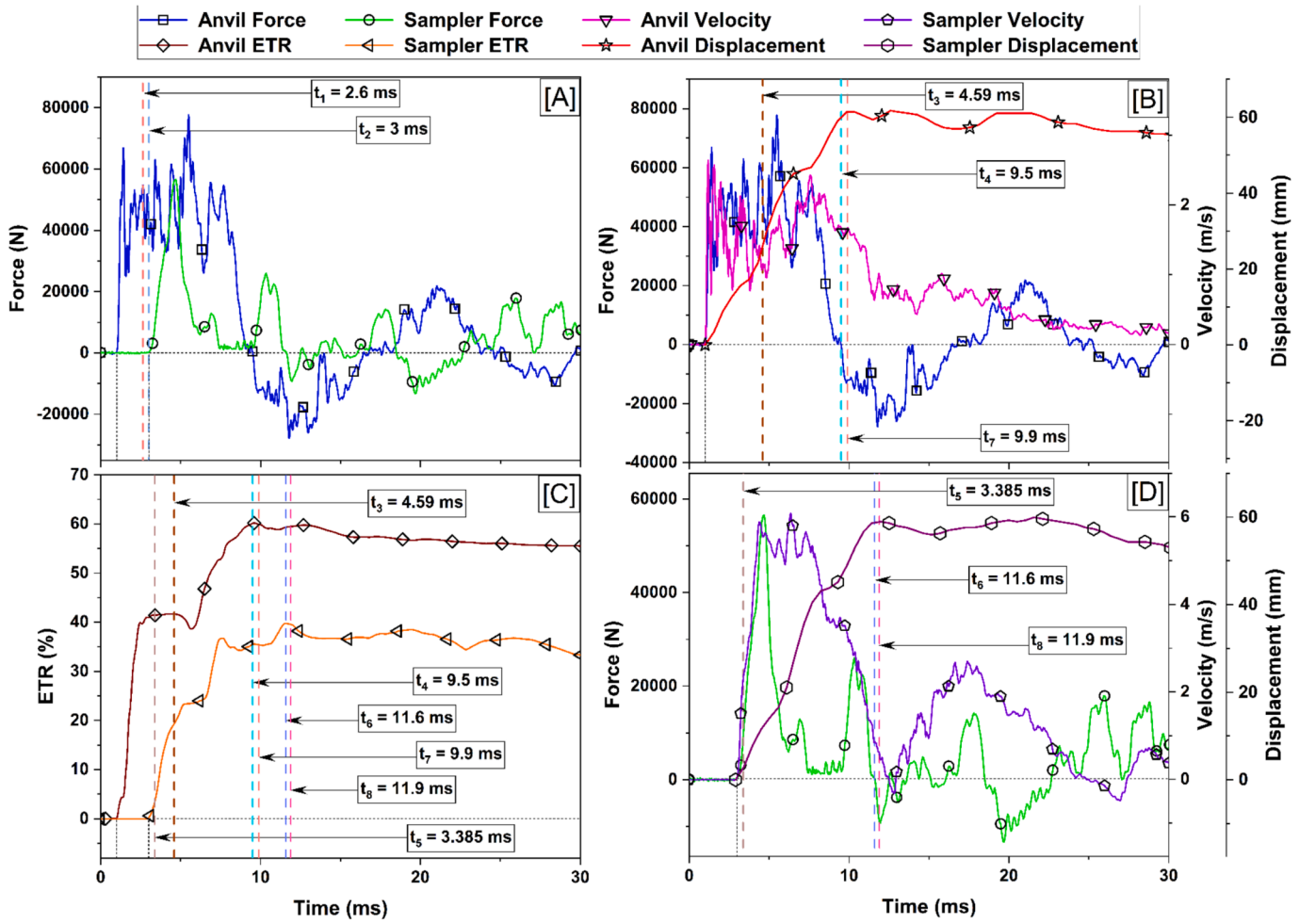

Fig. 18. Typical raw data time history plot of [A] Force at the anvil and sampler level, [B] force and velocity at the anvil level, [C] ETR at the anvil and sampler level, and [D] force and velocity at the sampler level for N value = 5 (i.e, penetration per blow = 60 mm).

offers a dynamic way to define the time window for calculating ETR in SPT. In this method, the ETR is calculated from the start of the stress wave until the point where either the force or the velocity changes direction from positive to negative, whichever happens first.

When the force rapidly changes its sign from positive to negative, it signifies the arrival of a significantly reflected tensile wave. This phenomenon typically occurs for N values less than 20, as shown in plots [B] and [D] of Fig. 18 and Fig. 19. Conversely, if the force magnitude is insignificant, it may not change sign promptly; it might gradually approach zero or sometimes even at the end of stress wave propagation. Such behaviour is common for N values $\geq$ 20, as observed in plots [B] and [D] of Figs. 20-23. The underlying reason lies in the specific impedance of the drill rod, which consistently exceeds that of the soil or rock. If the impedance ratio remains less than 1, reflected stress amplitudes and displacement are always smaller than the incident wave [34]. Consequently, the force–time history only changes direction from positive to negative when the magnitude of the reflected wave is significantly large, causing a rapid transition.

Alternatively, if the velocity changes sign from positive to negative, it indicates that the particle velocity at the measurement point has reversed its direction from downward to upward. This happens due to wave reflections during the impact. The FVCD method captures whichever of these two events (force or velocity sign change) occurs first, making it more adaptable and physically meaningful. In 1D wave propagation theory, a stress wave encountering an impedance discontinuity (e.g., joint or boundary) reflects a tensile wave that often reverses the direction of force or velocity. Building on this fundamental concept, the point at which this reversal first occurs marks the limit of effective energy transfer, beyond which additional integration may include unwanted reflected or dissipated energy components. This ensures that only the energy relevant to forward penetration is captured, while minimizing the influence of significant late-arriving reflected or dissipated components. Hence, the FVCD method uses this idea to find a more accurate and meaningful time duration for considering energy transfer in SPT.

Further, HSC with a circular target record is used to confirm this. When analysing the sensor-based SPT HEMA and visual-based HSC data at the anvil level, it was found that t_4 and t_7 time values are very close to each other, as shown in the plot [B] of Figs. 18-23. Similarly, for the sampler level, t_6 and t_8 time values are very close to each other, as shown in the plot [D] of Figs. 18-23. Hence, the FVCD method is more reliable, as it considers ETR to correspond to the actual sampler penetration duration. This method dynamically defines the time window based on actual wave behavior rather than using a fixed time window. Hence, the FVCD approach allows a comprehensive assessment of ETR to the drill rod by considering wave reflection and particle velocity. For better visualisation, all the summaries of Figs. 18-23 are grouped, compared, and explained together in the following section (*Section 3.3*).

3.3. Summary of laboratory studies

The summary of the analysis from Fig. 18 to Fig. 23 is shown in Table 3 and Fig. 24, as a comparative duration, and ETR analysis of time-dependent SPT-N value results with corresponding durations of anvil

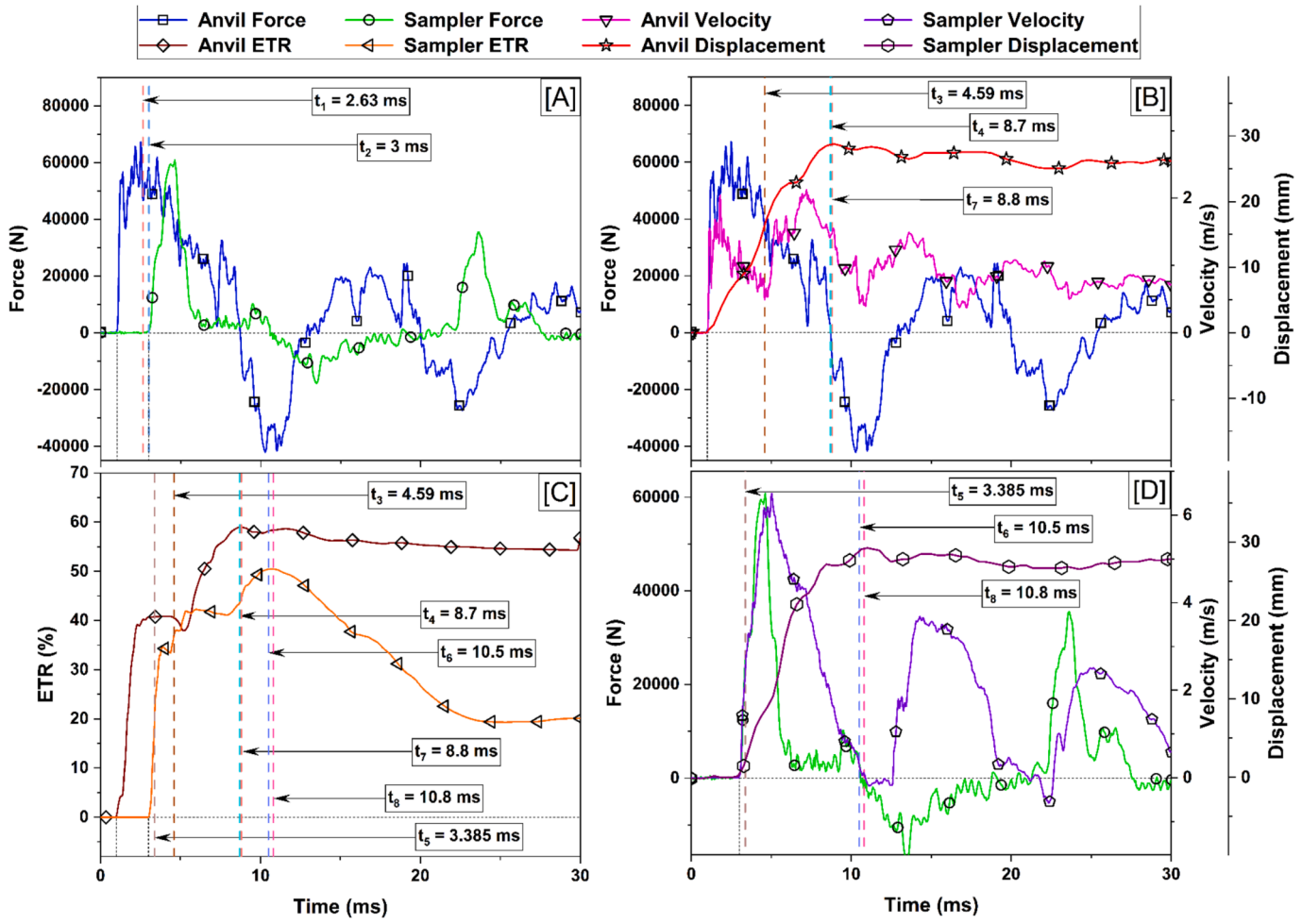

Fig. 19. Typical raw data time history plot of [A] force at the anvil and sampler level, [B] force and velocity at the anvil level, [C] ETR at the anvil and sampler level, and [D] force and velocity at the sampler level for N value = 10 (i.e, penetration per blow = 30 mm).

and sampler level measurements of force, velocity, ETR, and displacement.

If we observe Fig. 24*[A]*, we can see that the time durations t_4, t_6, t_7, and t_8 are higher when the N value is low, and gradually decrease as the N value increases. This happens because lower N values indicate weaker soils, which take more time to allow the sampler to fully penetrate and settle. In comparison, higher N values represent stiffer soils that resist penetration, resulting in quicker but shorter duration displacements. This is supported by the consistent decrease in t_7 and t_8 with increasing N values, indicating a direct correlation between penetration time and soil stiffness, which further supports FVCD and HSCCT methods. However, as t_3 and t_5 are constant across all N values, the FV method fails to adapt to changing soil resistance, highlighting the need for a dynamic time window such as FVCD.

The ETR is considered such that the peak ETR value is selected within the specified time frame, like t_3 to t_8. Fig. 24*[B]* shows that the maximum ETR values from t_4 and t_7 align well for anvil-level measurements, and similarly, t_6 and t_8 show close agreement for sampler-level measurements. This highlights a good match between sensor-based FVCD time windows and visually observed displacements from HSCCT.

Notably, the ETR values obtained using the FVCD method (t_4 and t_6 time windows) are significantly higher than those estimated by the traditional FV method (t_3 and t_5 time windows). This difference is most pronounced in the sampler ETR values using the FV method at t_5, where the energy captured is often around 50 % less than that of FVCD. Such underestimation is particularly severe in soft soils and short rod scenarios. When the rod length below the sensor is minimal, the '2L/c' time window is too short to capture the full energy transfer. In these cases, the ETR from the FV method may approach zero, which is not practically acceptable.

As the N value increases, the ETR difference between FV and FVCD becomes slightly smaller, but FV still consistently underestimates the energy compared to FVCD. The FVCD and HSCCT methods, especially at the sampler level (t_6 and t_8 time windows), capture much higher and more realistic ETR values, showing better consistency across different N values.

Overall, the FVCD method provides a more accurate and reliable energy measurement, regardless of N value, penetration depth, or rod length. It effectively addresses the limitations of previous studies, especially those involving short rods. The following sections will further explore the advantages of the FVCD method using a large laboratory and field SPT data dataset.

3.4. Comparison of FV and FVCD methods for large data sets

Following the detailed analysis of ETR behaviour across individual N values using selected cases, the FV and FVCD methods were further evaluated using a comprehensive dataset of laboratory and field SPT blows. Fig. 25 and Fig. 26 correspond to laboratory data, while Fig. 27 and Fig. 28 represent field data. Each dataset includes ETR values computed from both the conventional FV method and the proposed FVCD method.

Fig. 25 and Fig. 27 compare the Anvil ETR and Sampler ETR results

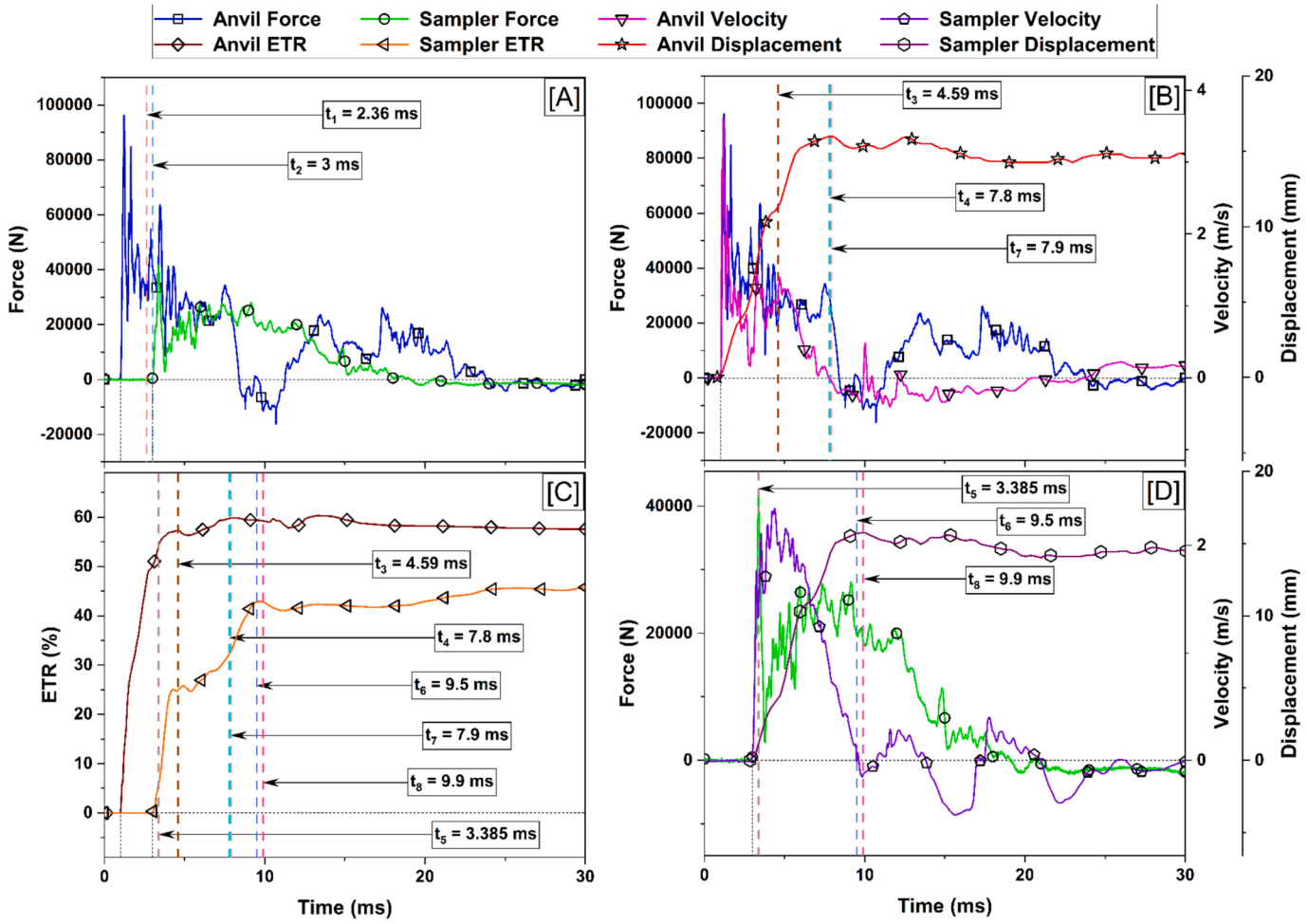

Fig. 20. Typical raw data time history plot of [A] force at the anvil and sampler level, [B] force and velocity at the anvil level, [C] ETR at the anvil and sampler level, and [D] force and velocity at the sampler level for N value = 20 (i.e, penetration per blow = 15 mm).

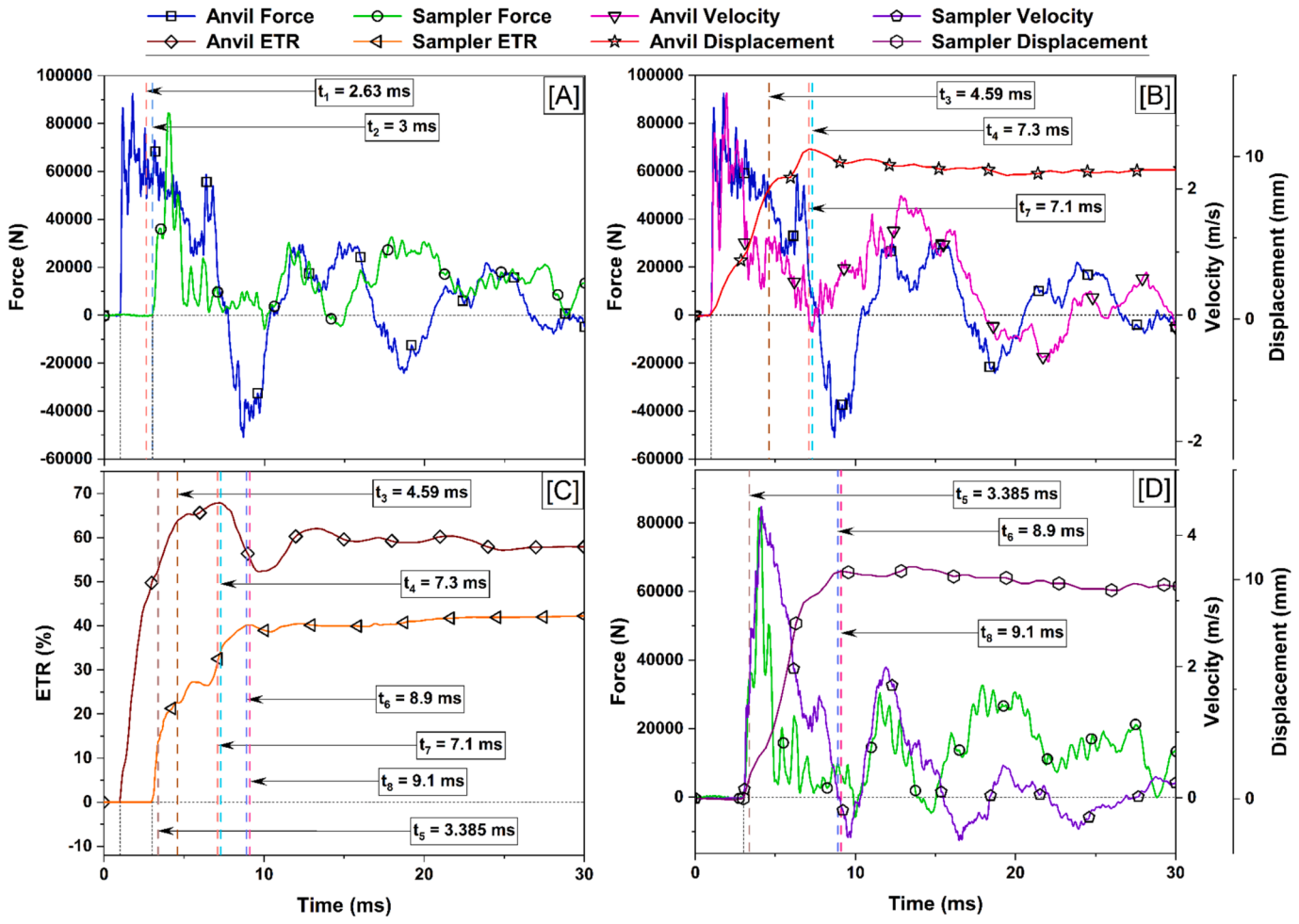

Fig. 21. Typical raw data time history plot of [A] force at the anvil and sampler level, [B] force and velocity at the anvil level, [C] ETR at the anvil and sampler level, and [D] force and velocity at the sampler level for N value = 30 (i.e, penetration per blow = 10 mm).

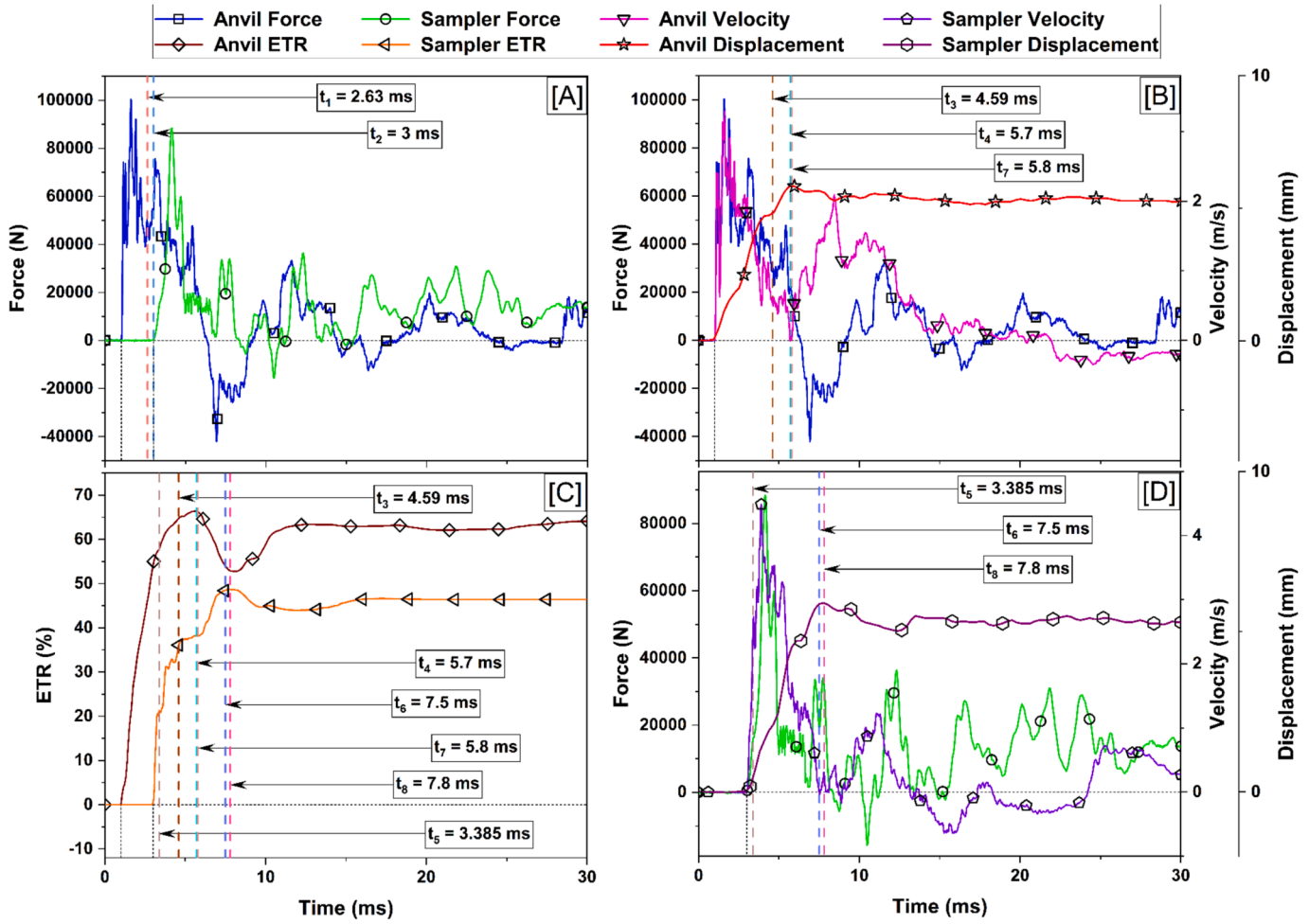

Fig. 22. Typical raw data time history plot of [A] force at the anvil and sampler level, [B] force and velocity at the anvil level, [C] ETR at the anvil and sampler level, and [D] force and velocity at the sampler level for N value = 50 (i.e, penetration per blow = 6 mm).

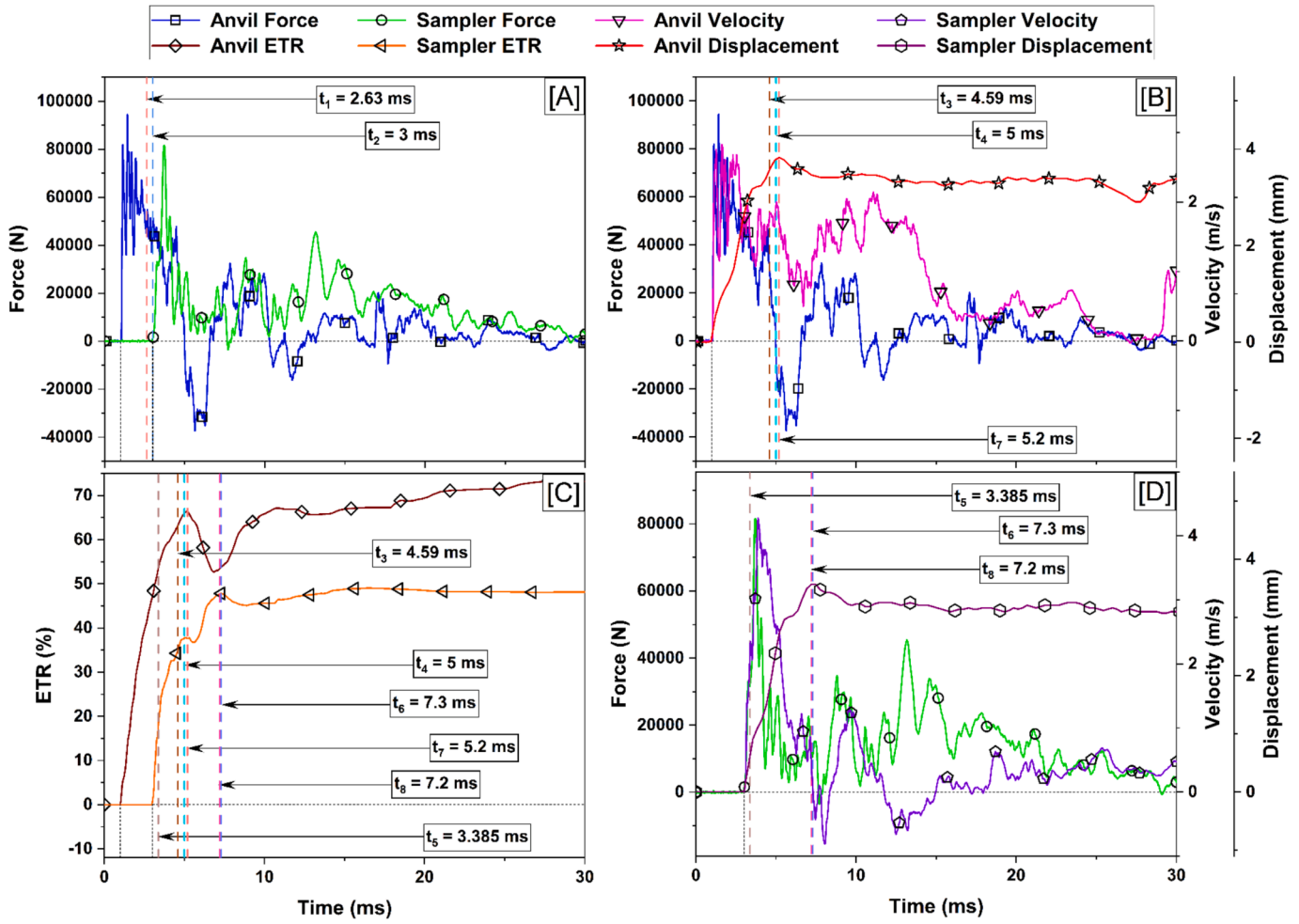

Fig. 23. Typical raw data time history plot of [A] force at the anvil and sampler level, [B] force and velocity at the anvil level, [C] ETR at the anvil and sampler level, and [D] force and velocity at the sampler level for N value = R or 100 (i.e, penetration per blow < 3 mm).

obtained using both methods. Plot [A] shows Anvil ETR, and plot [B] shows Sampler ETR, both plotted against the number of blows. Each data point represents one blow, and the two colored trendlines represent linear fits for each method. In both subplots, the green open circles represent the ETR values obtained using the FVCD method, while the orange crosses show those from the FV method. It can be seen that the ETR values obtained from the FVCD method are consistently higher and more stable than those from the FV method, especially at the sampler level. The gap between the two trendlines in plot [B] (Sampler ETR) is much larger than in plot [A] (Anvil ETR), confirming that the FV method underestimates sampler-level energy more significantly. These figures also show that FVCD maintains better consistency across all blow counts. In contrast, the FV method shows scattered and lower values, especially at lower blow counts, which is critical in short-rod or soft-soil scenarios.

To further compare the two methods statistically, Bland–Altman plots were generated for both laboratory and field datasets, as shown in Fig. 26 and Fig. 28, respectively. These plots are commonly used to visually assess the agreement between two measurement techniques. The x-axis represents the average of the ETR values from the FV and FVCD methods, and the y-axis shows the difference between them (FV − FVCD).

In Fig. 26 (laboratory data), plot [A] shows that the average difference in Anvil ETR between the two methods is approximately –3.5 %, while in plot [B], the difference in Sampler ETR is much higher at about –13.7 %. The dotted lines represent the limits of agreement, calculated as ± 1.96 times the standard deviation of the differences. These plots clearly show that the FV method consistently underestimates the ETR values compared to FVCD, and the bias is more pronounced at the sampler level. Similarly, Fig. 28 presents the Bland–Altman plots for field data. Plot [A] shows a mean difference of –4.2 % for Anvil ETR, while plot [B] reveals a larger bias of –8.8 % at the sampler level. The data spread in both plots again confirms that the discrepancy between FV and FVCD increases at lower ETR values, which is typical in soft soils or shallow depths.

These statistical comparisons reinforce that FVCD yields higher and more realistic ETR values and shows less variation and stronger agreement across different blow counts. Hence, FVCD offers a more accurate and consistent method for evaluating energy transfer, especially in critical cases such as low N values or short rod lengths.

Further, a detailed statistical comparison was carried out to evaluate the performance between the FV and FVCD methods. Table 4 presents a comparison of key statistical metrics for ETR values obtained using the FV and FVCD methods in laboratory and field SPTs, measured at the anvil and sampler levels. The table shows common descriptive statistics such as the mean, standard deviation (SD), median, and range, which describe the spread and central value of the ETR data. The table also shows measures like standard error, confidence intervals (CI), and p-values to assess the reliability of the differences.

The FVCD method gives a higher mean ETR than the FV method in all cases. All p-values are 0, meaning the improvements seen with the FVCD method are statistically significant. The 95 % confidence intervals for FVCD are consistently higher, further supporting its accuracy. In addition, the Cohen's d_s values are all moderately to strongly negative,

Table 3
Comparative duration and ETR analysis for time-dependent SPT-N value results with respect to corresponding anvil and sampler level measurements of force, velocity, ETR, and displacement.

N value	Penetration per blow (mm)	t_1 (L_1/c, Theoretical arrival time at sampler)	t_2 (measured arrival time at sampler)	t_3 ($2L_5$/c, FV method – anvil)	ETR @ t_3 ([4,12,13])	t_4 (FVCD method – anvil)	ETR @ t_4	t_5 ($2L_5$/c, FV method – sampler)	ETR @ t_5 ([17,18,19])	t_6 (FVCD method – sampler)	ETR @ t_6	t_7 (HSC peak disp – anvil)	ETR @ t_7	t_8 (HSC peak disp – sampler)	ETR @ t_8
5	60	2.63	3	4.59	41.8	9.5	60	3.385	4	11.6	39.7	9.9	60	11.9	39.7
10	30	2.63	3	4.59	40.8	8.7	59	3.385	19	10.5	50.8	8.8	59	10.8	50.8
20	15	2.63	3	4.59	56.6	7.8	59.9	3.385	6	9.5	42.7	7.9	59.9	9.9	42.7
30	10	2.63	3	4.59	64	7.3	67.6	3.385	13.5	8.9	40	7.1	67.6	9.1	40
50	6	2.63	3	4.59	64.9	5.7	66.3	3.385	21	7.5	48	5.8	66.3	7.8	48.3
100	3	2.63	3	4.59	64	5	66	3.385	17	7.3	47.4	5.2	66.2	7.2	47.5

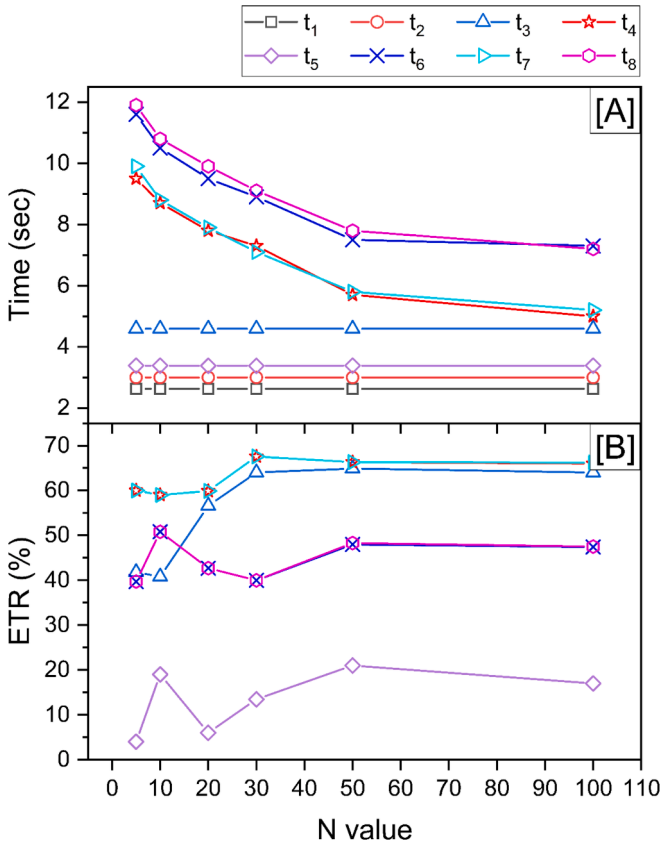

Fig. 24. Comparative [A] duration and [B] ETR analysis of time-dependent SPT-N value results with corresponding durations of anvil and sampler level measurements of forces, Velocities, ETR, and displacement.

which means the FVCD method is not only statistically better but also practically meaningful, with a difference significant enough to make a real impact. The SD difference and pooled SD also confirm that FVCD results are more consistent and less biased, especially at the sampler level, where accurate energy measurement is critical. Overall, Table 4 confirms that the FVCD method provides higher and reliable ETR values, both in controlled laboratory conditions and real field conditions.

These larger data set comparisons support the trends in the earlier detailed cases and show that the FVCD method works well under different testing conditions. Compared to earlier studies such as Odebrecht et al. and Lukiantchuki et al. [17,18], which reported conflicting or unclear observations about sampler-level energy, the current study provides a more consistent and validated method for estimating ETR using a broader dataset. Additionally, while Hong et al. [19] presented ETR value at the sampler level, the specific time window used for energy calculation was not mentioned. The reported duration appears to align with a short '2L/c' window. However, this study shows that such a window is often insufficient for complete energy accumulation at the sampler level, especially in short rod cases. As a result, the reported energy values may underestimate the actual energy transfer. In contrast, the FVCD method defines a more appropriate time window. This approach is further validated through displacement measurements, offering improved accuracy in sampler-level energy estimation. These results emphasize the reliability and applicability of the extended time window FVCD method across various N values and drill rod lengths, especially in cases of short rod lengths.

4. Conclusion

This paper presents a novel and robust approach, the Force or Velocity Change Direction (FVCD) method, for reliable hammer energy

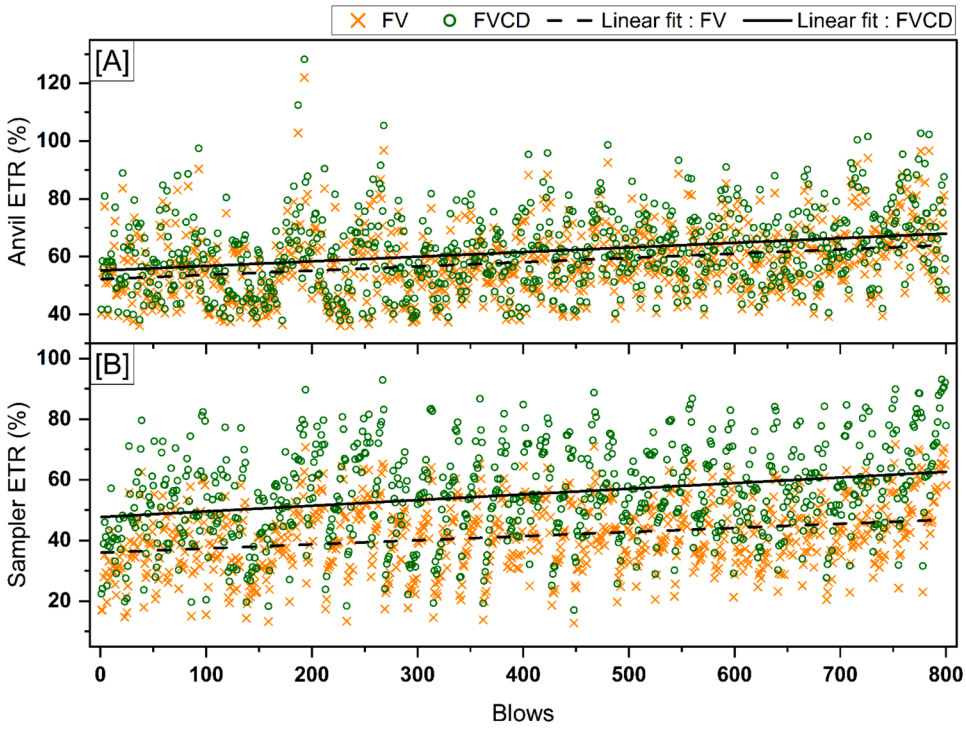

Fig. 25. Comparison of Anvil and Sampler ETR results of laboratory SPT obtained from FV and FVCD methods.

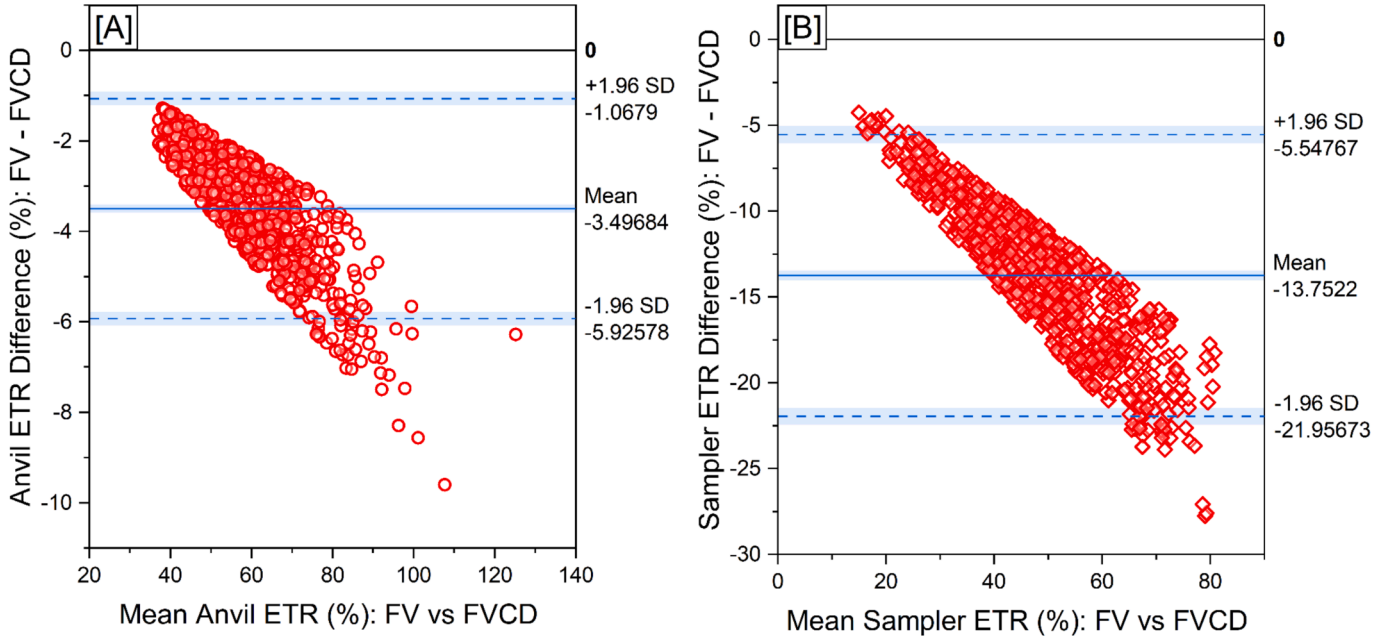

Fig. 26. Bland-Altman plots for laboratory SPT data comparing ETR values obtained from FV and FVCD methods at (a) anvil level and (b) sampler level.

measurement in Standard Penetration Tests (SPT). Extensive field (89 boreholes, 492 SPTs, 19,493 blows) tests were conducted under various rig types, hammer mechanisms, depths, and soil conditions. Additionally, extensive full-scale SPT laboratory tests (44 SPTs, 838 blows) were conducted in a controlled environment. The study employed the SPT HEMA system for hammer energy measurement at both anvil and sampler levels. Additionally, a High-Speed Camera with circular target marks (HSCCT) captured the anvil and sampler movement in the full-scale controlled laboratory SPT model setup. The FVCD method considers ETR from the start of the waveform until either the force or velocity changes its sign from positive to negative, whichever occurs first. The force sign change corresponds to significant reflected waves, while the velocity sign change indicates the change in particle direction or forward-moving tensile stress, resulting in negative velocity. The extended time window FVCD method was found to be the most reliable and applicable approach across various N values and drill rod lengths, especially in cases involving short rods. Non-contact energy measurements using the HSCCT technique were compared with the FV and FVCD methods. The ETR values from FVCD closely matched those from HSCCT at both the anvil and sampler levels, while the FV method showed poor

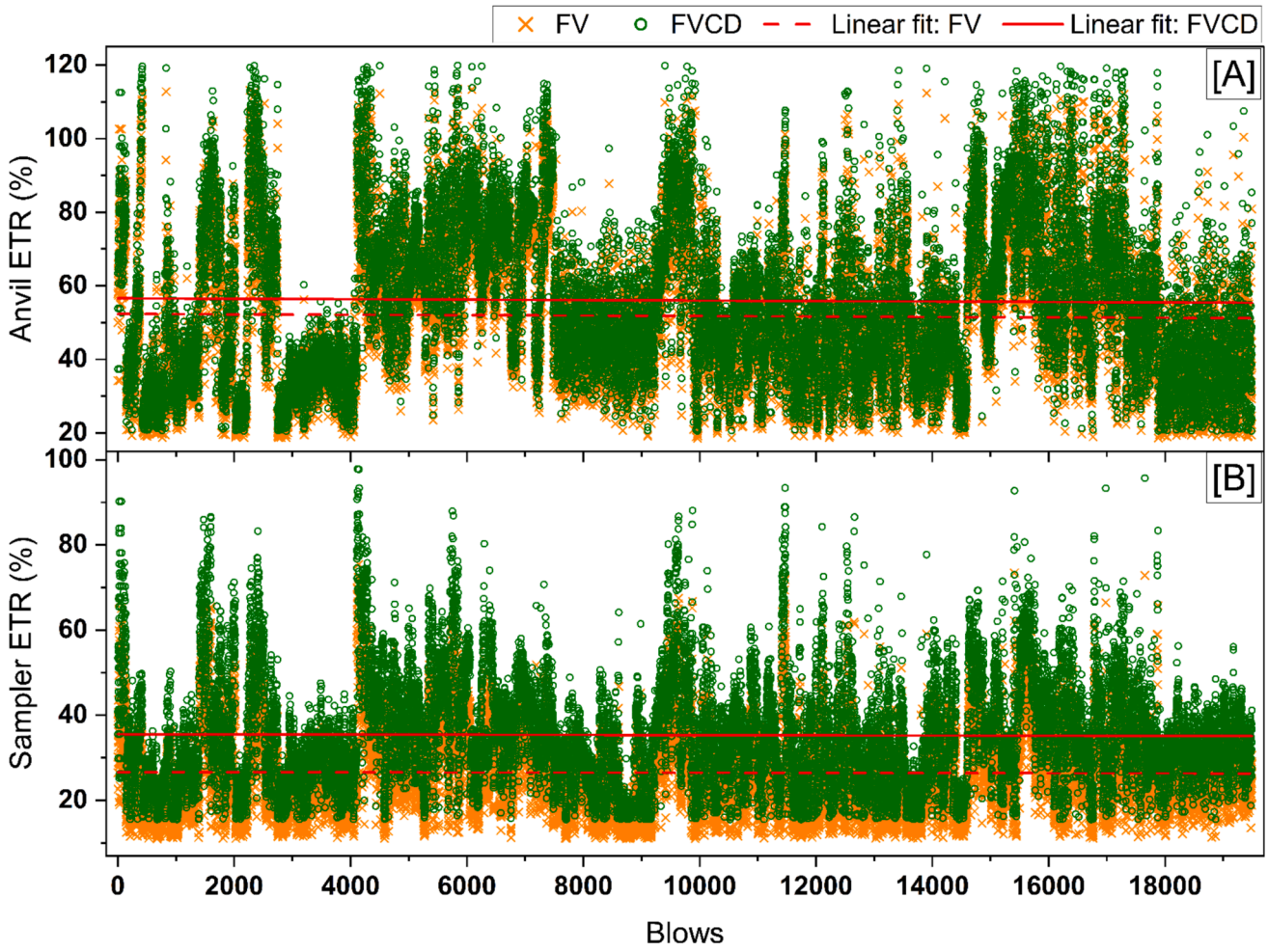

Fig. 27. Comparison of Anvil and Sampler ETR results of Field SPT obtained from FV and FVCD methods.

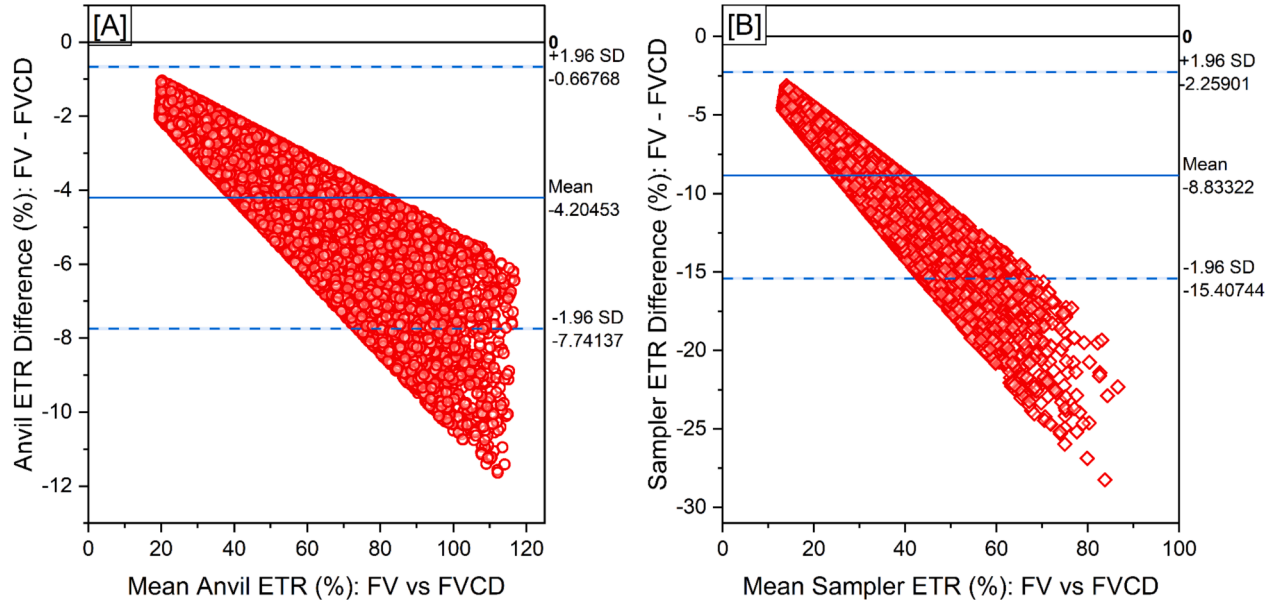

Fig. 28. Bland-Altman plots for field SPT data comparing ETR values obtained from FV and FVCD methods at (a) anvil level and (b) sampler level.

agreement. This work is the first to propose a dynamic, sign-based time window for ETR estimation, validated across large-scale field and lab datasets. The FVCD method provides a more reliable ETR measurement regardless of the N value, rod length, penetration duration, and penetration depth. This shows that the FVCD approach is more reliable, consistent, and capable of producing accurate energy measurements.

Table 4
Statistical comparison of FV and FVCD methods for SPT ETR (%) in laboratory and field datasets.

Data Category	Laboratory SPT ETR (%) data set				Field SPT ETR (%) data set			
	Anvil		Sampler		Anvil		Sampler	
	FV	FVCD	FV	FVCD	FV	FVCD	FV	FVCD
Mean	58	62	41	55	52	56	26	35
Standard Error	0.43	0.47	0.41	0.54	0.14	0.15	0.07	0.09
Median	57	61	41	55	48	52	25	33
SD	12.2	13.3	11.7	15.4	19.5	21.0	9.5	12.6
Sample Variance	149	176	136	237	379	442	91	160
Kurtosis	0.82	0.78	−0.42	−0.46	−0.40	−0.42	1.02	0.99
Skewness	0.65	0.66	0.05	0.03	0.57	0.56	0.94	0.94
Range	86	90	59	76	95	99	64	82
Minimum	36	38	13	17	19	21	11	16
Maximum	122	128	72	93	113	120	75	98
Count	838	838	838	838	19,493	19,493	19,493	19,493
Upper CI (95 %)	58.9	62.5	42.2	56.3	51.9	56.3	26.7	35.6
Lower CI (95 %)	57.2	60.7	40.6	54.1	51.6	55.7	26.3	35.0
Mean difference (FV − FVCD)	−3.50		−13.75		−4.20		−8.83	
SD difference (FV − FVCD)	1.24		4.19		1.80		3.35	
P value (FV − FVCD)	0		0		0		0	
Pooled SD (FV − FVCD)	12.8		13.7		20.3		11.2	
Cohen's d_s (FV − FVCD)	−0.27		−1.01		−0.21		−0.79	

The proposed FVCD method significantly enhances the reliability of energy transfer measurement in SPT and can lead to more consistent assessments of soil behaviour and penetration resistance in geotechnical engineering.

However, this study also has a few limitations. The method's accuracy depends on the quality of force and acceleration data. Minor noise or misalignment in sensors may affect results. However, no such issues were observed in this study's field or laboratory tests. Further investigation may be needed under extreme or uncommon testing conditions (such as very deep boreholes, non-standard SPT setups, or offshore SPTs). The FVCD method was applied to data collected using a wide range of rigs, rod types, and soil profiles commonly encountered in India. However, additional validation may be required for unusual or highly variable geotechnical conditions (such as collapsible soils, highly stratified and heterogeneous soil layers, or offshore SPTs) where the wave reflections might be complex.

Future work can explore how the FVCD method is affected by the individual effects of different rig types, hammer systems, rod types, and soil conditions on energy transfer during SPT. In addition to field and lab studies, numerical modelling could simulate wave behaviour and validate energy transfer mechanisms under controlled conditions. Additionally, future studies may explore integrating with machine learning models for predictive analysis and advanced signal processing techniques, such as wavelet analysis, to enhance the understanding of energy transfer efficiency.

Funding details

This work was supported by the SERB, DST, Govt. of India for the project "Development of correction factors for standard penetration test N values in India through energy measurement and field experiments – Step towards a reliable Liquefaction Potential Assessment" under Grant SERB/F/198/2017–18 dated 11/05/2017; and Dam Safety (Rehabilitation) Directorate, Central Water Commission (CWC) for funding the "International Centre of Excellence in Dam Engineering" (ICoEDE) under the Dam Rehabilitation and Improvement Project (DRIP); Ministry of Jal Shakti (MoJS), Government of India for the project entitled "Integrated Investigation for Risk Assessment of the Dam" under grant R-24011/57/2023-Pen Riv Section-MOWR.

CRediT authorship contribution statement

M.E. Yadhunandan: Writing – original draft, Visualization, Validation, Software, Methodology, Investigation, Formal analysis, Data curation, Conceptualization. **Panjamani Anbazhagan:** Writing – original draft.

Declaration of competing interest

The authors declare that they have no known competing financial interests or personal relationships that could have appeared to influence the work reported in this paper.

Acknowledgements

The authors thank Mr. Silas, Research Scholar, Department of Civil Engineering, Indian Institute of Science, for his valuable input on wave propagation. The authors also thank Mr. Harsh, Mr. Suhas, Mr. Dinesh, and Ms. Yaksha, internship students in the same department, for their valuable assistance during SPT testing.

Data availability

Data is available in the form of Excel spreadsheets and is available from the corresponding author upon reasonable request.

References

[1] Y. Lacroix, H. Horn, Direct Determination and indirect Evaluation of Relative Density and its use on Earthwork Construction Projects, West Conshohocken, PA: ASTM International 1973 (Jan. 1973) 251–280, https://doi.org/10.1520/STP37877S.
[2] ASTM Standard D3740-19 Standard practice for minimum requirements for agencies engaged in testing and/or inspection of soil and rock as used in engineering design and construction, West Conshohocken, PA, USA., 2019. doi: 10.1520/D3740-19.
[3] BIS 2131, Method for standard penetration test for soils, reaffirmed 2021, Bureau of Indian Standards, New Delhi., 1981, p. 1981.
[4] ASTM Standard D4633-16 - Standard Test Method for Energy Measurement for Dynamic Penetrometers, West Conshohocken, PA, USA., 2016. doi: 10.1520/D4633-16.
[5] BS EN ISO 1377-9:1990 - soils for engineering purposes—insitu tests., London, UK., 1990.
[6] BIS 9640, Indian standard specification for split spoon sampler, reaffirmed 2007, Bureau of Indian Standards, New Delhi., 1980, p. 1980.
[7] BIS 1893 (Part 1) : 2016 - Criteria for Earthquake Resistant Design of Structures, Bureau of Indian Standards, New Delhi., 2016.
[8] P. Anbazhagan, K. Ayush, M.E. Yadhunandan, K. Siriwanth, K. Suryanarayana, G. Sahodar, Effective use of SPT: hammer energy measurement and integrated subsurface investigation, Indian Geotech J 52 (5) (Oct. 2022) 1079–1096, https://doi.org/10.1007/s40098-022-00609-z.

[9] P. Anbazhagan, M.E. Yadhunandan, A. Kumar, Effects of Hammer Energy on borehole termination and SBC calculation through site-specific hammer energy measurement using SPT HEMA, Indian Geotech J 52 (2) (Apr. 2022) 381–399, https://doi.org/10.1007/s40098-021-00582-z.
[10] W. Kovacs, E. Jc, and G. Ah, "Towards a more standardized SPT.," 1977, Accessed: Apr. 22, 2025. [Online]. Available: http://pascal-francis.inist.fr/vibad/index.php?action=getRecordDetail&idt=PASCALGEODEBRGM7820362277.
[11] J.H. Schmertmann, A. Palacios, Energy Dynamics of SPT, J. Geotech. Eng. Div. 105 (8) (Aug. 1979) 909–926, https://doi.org/10.1061/AJGEB6.0000839.
[12] A. Sy, R.G. Campanella, "An Alternate Method of Measuring SPT Energy," presented at the International Conferences on Recent Advances in Geotechnical earthquake engineering and soil dynamics, Mar. 1991. [Online]. Available: https://scholarsmine.mst.edu/icrageesd/02icrageesd/session03/2/.
[13] H. Abou-matar, G.G. Goble, SPT dynamic analysis and measurements, J. Geotech. Geoenviron. Eng. 123 (10) (Oct. 1997) 921–928, https://doi.org/10.1061/(ASCE)1090-0241(1997)123:10(921).
[14] H. Bolton Seed, K. Tokimatsu, L. F. Harder, and R. M. Chung, Influence of SPT procedures in soil liquefaction resistance evaluations, J. Geotech. Engrg. 111(12) (1985) 1425–1445. doi: 10.1061/(ASCE)0733-9410(1985)111:12(1425).
[15] C.M. Morgano, R. Liang, Energy transfer in SPT – Rod length effect. Application of stress-wave theory to piles, Routledge, 1992.
[16] K.O. Cetin, M.E. Cevik, A. Al-Suhaily, A.A. Yunatci, Probabilistic Assessment of Standard Penetration Test Hammer energy efficiency and rod length corrections, J. Geotech. Geoenviron. Eng. 149 (8) (Aug. 2023) 04023055, https://doi.org/10.1061/JGGEFK.GTENG-11136.
[17] E. Odebrecht, F. Schnaid, M. M. Rocha, G. De Paula Bernardes, Energy efficiency for standard penetration tests, J. Geotech. Geoenviron. Eng. 131(10) (2005): 1252–1263. doi: 10.1061/(ASCE)1090-0241(2005)131:10(1252).
[18] J.A. Lukiantchuki, G.D.P. Bernardes, E.R. Esquivel, Energy ratio (ER) for the standard penetration test based on measured field tests, SR 40 (2) (Aug. 2017) 77–91, https://doi.org/10.28927/SR.402077.
[19] W.-T. Hong, S.Y. Kim, J.-S. Lee, Evaluation of driving energy transferred to split spoon sampler for accuracy improvement of standard penetration test, Measurement 188 (Jan. 2022) 110384, https://doi.org/10.1016/j.measurement.2021.110384.
[20] E. Odebrecht, F. Schnaid, M.M. Rocha, and G. de Paula Bernardes, "Energy Efficiency for Standard Penetration Tests," J. Geotechn. Geoenviron. Eng. 131(10), pp. 1252–1263, Oct. 2005. doi: 10.1061/(ASCE)1090-0241(2005)131:10(1252).
[21] H. Abou-matar, "Evaluation of dynamic measurements on the standard penetration test," Thesis presented to the University of Colorado at Boulder in partial fulfillment of the degree of MS, 1990, [Online]. Available: https://cir.nii.ac.jp/crid/1570572700170453632.
[22] J. A. Howie, C. R. Daniel, R. S. Jackson, B. Walker, and A. Sy, "Comparison of energy measurement methods in the standard penetration test : final report, appendices I, II, III, and IV." Accessed: Apr. 23, 2025. [Online]. Available: https://open.library.ubc.ca/soa/cIRcle/collections/facultyresearchandpublications/52383/items/1.0048557.
[23] C. Lee, S. An, W. Lee, Real-time monitoring of SPT donut hammer motion and SPT energy transfer ratio using digital line-scan camera and pile driving analyzer, Acta Geotech. 9 (6) (Dec. 2014) 959–968, https://doi.org/10.1007/s11440-012-0197-0.
[24] J. B. Anderson and J. N. Honeycutt, "Energy Calibration for Aldot Standard Penetration Test Equipment and Operators," Auburn Umiversity, Alabama 36849, IR 10-02, Jul. 2021. [Online]. Available: https://www.eng.auburn.edu/files/centers/hrc/ir-10-02-anderson-energy-calibration.pdf.
[25] J. A. Farrar, "Summary of standard penetration test (SPT) energy measurement experience," in Geotechnical site characterization, 1998, pp. 919–926. [Online]. Available: http://pascal-francis.inist.fr/vibad/index.php?action=getRecordDetail&idt=6214128.
[26] C.R. Daniel, J.A. Howie, R.S. Jackson, B. Walker, Review of Standard Penetration Test Short Rod Corrections, J. Geotech. Geoenviron. Eng. 131 (4) (Apr. 2005) 489–497, https://doi.org/10.1061/(ASCE)1090-0241(2005)131:4(489).
[27] E.H. Cavalcante, F.A.B. Danziger, B.R. Danziger, Estimating the SPT penetration resistance from rod penetration based on instrumentation, Geotech. Geophys. Site Character. (2004) 293–298.
[28] C.M. Santana, F.A.B. Danziger, B.R. Danziger, Energy measurement in the Brazilian SPT System, S&R 37 (3) (Sep. 2014) 243–255, https://doi.org/10.28927/SR.373243.
[29] C. Lee, J.-S. Lee, S. An, W. Lee, Effect of secondary impacts on spt rod energy and sampler penetration, J. Geotech. Geoenviron. Eng. 136 (3) (Mar. 2010) 522–526, https://doi.org/10.1061/(ASCE)GT.1943-5606.0000236.
[30] S.-N. Lee, B.-J. You, M.-S. Limb, S.-R. Oh, S.-S. Han, and S. H. Lee, "Visual measurement of pile penetration and rebound movement using a high-speed line-scan camera," in Proceedings 2002 IEEE International Conference on Robotics and Automation (Cat. No. 02CH37292), IEEE, 2002, pp. 4307–4312. [Online]. Available: https://ieeexplore.ieee.org/abstract/document/1014436/.
[31] M.-S. Lim, B.-J. You, S.-R. Oh, S.-S. Han, and S.-H. Lee, "Visual Precise Measurement of Pile Rebound and Penetration Movement Using a High-Speed Line-Scan Camera," Transactions on Control, Automation and Systems Engineering, vol. 4, no. 4, pp. 341–346, 2002, Accessed: Apr. 23, 2025. [Online]. Available: https://koreascience.kr/article/JAKO200211921518888.page.
[32] M.E. Yadhunandan, P. Anbazhagan, Effective visual measurement system for SPT hammer energy measurement, Measurement (2025) 117777, https://doi.org/10.1016/j.measurement.2025.117777.
[33] K. H. Miller, "An investigation of standard penetration test hammer efficiency through measurement of impact velocity and stress wave energy," PhD Thesis, University of British Columbia, 2022. [Online]. Available: https://open.library.ubc.ca/soa/cIRcle/collections/ubctheses/24/items/1.0413223.
[34] S.L. Kramer, Geotechnical Earthquake Engineering, University of Washington, 1996.